Chemical Geology 500 (2018) 1–19

Contents lists available at ScienceDirect

Chemical Geology

journal homepage: www.elsevier.com/locate/chemgeo

Invited research article

Olivine dissolution rates: A critical review

Eric H. Oelkers[a,b,*], Julien Declercq[c], Giuseppe D. Saldi[a,d], Sigurdur R. Gislason[b], Jacques Schott[a]

[a] Geoscience and Environment Toulouse (GET), CNRS, UMR 5563, Observatoire Midi-Pyrénées, 14 Avenue Edouard Belin, 31400 Toulouse, France
[b] Institute of Earth Sciences, University of Iceland, Sturlugata 7, 101 Reykjavik, Iceland
[c] SRK Consulting, Church House, 17 Churchill Way, Cardiff CF12 2HH, Wales, United Kingdom
[d] Earth Sciences, University College London, Gower Street, London WC1E 6DT, United Kingdom

ARTICLE INFO

Editor: Michael E. B

Keywords:
Forsterite dissolution
Mineral carbonation
Stable Mg isotopes
Enhanced weathering

ABSTRACT

The dissolution rates of olivine have been considered by a plethora of studies in part due to its potential to aid in carbon storage and the ease in obtaining pure samples for laboratory experiments. Due to the relative simplicity of its dissolution mechanism, most of these studies provide mutually consistent results such that a comparison of their rates can provide insight into the reactivity of silicate minerals as a whole. Olivine dissolution is controlled by the breaking of octahedral M^{2+}-oxygen bonds at or near the surface, liberating adjoining SiO_4^{4-} tetrahedra to the aqueous fluid. Aqueous species that adsorb to these bonds apparently accelerate their destruction. For example, the absorption of H^+, H_2O and, at some conditions, selected aqueous organic species will increase olivine dissolution rates. Nevertheless, other factors can slow olivine dissolution rates. Notably, olivine dissolution rates are slowed by lowering the surface area exposed to the reactive aqueous fluid, by for example the presence and/or growth on these surfaces of either microbes or secondary phases. The degree to which secondary phases decelerate rates depends on their ability to limit access of the reactive aqueous fluids to the olivine surface. It seems likely that these surface area limiting processes are very significant in natural systems, lowering olivine surface reactivity in many environments compared to rates measured on cleaned surfaces in the laboratory.

A survey of the literature suggests that the major factors influencing forsteritic olivine dissolution rates are 1) pH, 2) water activity, 3) temperature, and 4) mineral-fluid interfacial surface area. Evidence suggests that the effects of aqueous inorganic and organic species are relatively limited, and may be attributed at least in part to their influence on aqueous solution pH. Moreover, the observed decrease in rates due to the presence of secondary mineral coatings and/or the presence of microbes can be attributed to their ability to decrease olivine surface area directly exposed to the reactive aqueous fluid. As the reactivity of forsterite surfaces are spatially heterogeneous, its surface area normalized rates will tend to decrease as it dissolves even in the absence of a mineral or bacterial coating. Each of these factors limits and or influences the application of forsterite dissolution to 1) enhanced weathering efforts, 2) mineral carbonation, and 3) the low temperature generation of hydrogen or hydrocarbons via the oxidation of its divalent iron.

1. Introduction

This review of the reactivity of olivine in aqueous solution has been motivated by a number of reasons. First, there have been more experimental investigations of the reactivity of olivine than any other multi-oxide silicate mineral, and over far wider experimental conditions. Moreover, the starting materials for most of these studies are close to or exactly identical. Many experimental studies have been focused on San Carlos Olivine, due to its widespread availability or similarly compositioned material, specifically olivine having ~10% Fe(II) in its divalent metal site. Moreover, as noted by Velbel (2009), the corrosion textures of naturally weathered olivines from various igneous and metamorphic parent rock bodies are similar, suggesting that this mineral weathers in the same manner regardless of its crystallization and/or recrystallization history. Consequently, in contrast with most other minerals, olivine reactivities measured in different studies and using distinct experimental methods tend to be consistent with one another.

A second major reason to review olivine dissolution rates is that its reactivity is relatively simple. Its structure is comprised of isolated

* Corresponding author at: Geoscience and Environment Toulouse (GET), CNRS, UMR 5563, Observatoire Midi-Pyrénées, 14 Avenue Edouard Belin, 31400 Toulouse, France.
E-mail address: ucfbeoe@ucl.ac.uk (E.H. Oelkers).

https://doi.org/10.1016/j.chemgeo.2018.10.008
Received 28 June 2018; Received in revised form 5 October 2018; Accepted 6 October 2018
Available online 09 October 2018
0009-2541/

$Si-O_4^{4-}$ tetrahedra linked by divalent cations. As such, its dissolution mechanism is less complex than most other naturally occurring multi-oxide silicates (Oelkers, 2001a). As there are no Si-O-Si linkages in its structure, significant leached layers are not commonly formed on olivine surfaces during dissolution. Moreover, olivine is highly thermodynamically unstable in ambient temperature aqueous solutions. As a consequence, ambient temperature water-olivine interaction studies are almost exclusively limited to dissolution studies performed in highly undersaturated solutions; dissolution rates at such conditions do not tend to be influenced by an approach of the fluid composition towards equilibrium with the dissolving olivine. Taking these various factors into account suggests that a detailed review of the ambient temperature dissolution behavior of olivine could provide new insights into the dissolution behaviors of the silicate minerals in general.

The reactivity of forsteritic olivine[1] and its aqueous alteration products has received increasing attention as a potential source material for the divalent cations required to carbonate CO_2 during carbon storage efforts (e.g. Giammar et al., 2005; Oelkers and Schott, 2005; Bearat et al., 2006; Matter et al., 2007; Oelkers et al., 2008a; Dufaud et al., 2009; Prigiobbe et al., 2009; Matter and Kelemen, 2009; King et al., 2010, 2011; Beinlich and Austrheim, 2012; Daval et al., 2011; Guyot et al., 2011; Klien and Garrido, 2011; Kohler et al., 2013; Gislason and Oelkers, 2014; Sissmann et al., 2013, 2014; Zhu et al., 2016; Li et al., 2018). Further recent interest in olivine dissolution rates stems from its potential role in the weathering of the Martian surface (e.g. Stopar et al., 2006; Olsen and Rimstidt, 2007; Hausrath et al., 2008; Hausrath and Brantley, 2010; Dehouck et al., 2014; Velbel, 2014; Olsen et al., 2015; Niles et al., 2017). Such interest has led to a large number of studies aimed at characterizing forsterite dissolution behavior and rates at various fluid compositions and temperatures (e.g. Luce et al., 1972; Sanemasa et al., 1972; Bailey, 1974; Grandstaff, 1978, 1986; Eriksson, 1982; Murphy and Helgeson, 1987, 1989; Blum and Lasaga, 1988; Van Herk et al., 1989; Banfield et al., 1990; Wogelius and Walther, 1991, 1992; Casey and Westrich, 1992; Seyama et al., 1996; Awad et al., 2000; Chen and Brantley, 2000; Rosso and Rimstidt, 2000; Pokrovsky and Schott, 2000a, 2000b; Oelkers, 2001b; Giammar et al., 2005; Golubev et al., 2005; Hänchen et al., 2006; Olsen and Rimstidt, 2008; Davis et al., 2009; Beinlich and Austrheim, 2012; Rimstidt et al., 2012; Olsson et al., 2012; Plümper et al., 2012; Wang and Giammar, 2012; Declercq et al., 2013; Garcia et al., 2013; Saldi et al., 2013; Van Noort et al., 2013; Bundeleva et al., 2014; Johnson et al., 2014; King et al., 2011, 2014; Martinez et al., 2014; Torres et al., 2014; Agrawal and Mehra, 2016). Further studies have defined the spatial and textural relationship between weathering olivine and its alteration products (e.g. Eggleton, 1984; Banfield et al., 1990; Zakaznova-Herzog et al., 2008; Velbel, 2009).

A number of recent studies have regressed the existing forsterite dissolution rate data to generate equations describing these rates a function of pH and temperature (e.g. Rimstidt et al., 2012; Crundwell, 2014). To avoid duplication, the present study is focused on identifying the relative influence of other, perhaps less well constrained factors including surface area, mineral coatings and the presence of microbial species on the overall dissolution behavior of olivine surfaces. The purpose of the present communication is to take advantage of the large number of studies aimed at forsterite surface reactivity to illuminate the effect of various processes on olivine dissolution rates.

2. Theoretical background

A mineral's structure is key to its reactivity as it defines 1) the bonds that need to be broken for its dissolution and 2) the identity of elements located at its surface as a function of crystal orientation. Olivine is composed of SiO_4^{4-} anions and Me^{2+} cations with a 1:2 M ratio of Si:Me. A major structural feature of olivine is that these Me^{2+} cations are situated in octahedral chains that run parallel to the c-axis (see Brown, 1980; Putnis, 1992). A schematic illustration of the olivine structure viewed along the a-axis is reported in Fig. 1. Each oxygen atom is bonded to the silicon by a single covalent bond. The four oxygen atoms have a partial negative charge because of these covalent bonds. Each of the four oxygen atoms of the SiO_4^{4-} anions is bonded to the divalent cations by an ionic bond. As such there are no Si−O−Si units in this structure. The cations occupy two different octahedral sites, which are commonly identified, as the M1 and M2 sites. The M2 site is larger and more regular than M1. The name of each olivine is determined by the identity of the dominant divalent metal cation in its structure. For example Mg olivine is forsterite, Fe olivine is fayalite, and Mn olivine is tephorite. Forsterite and fayalite form a complete solid solution, but the most common composition of olivine found on the surface of the Earth is a forsterite-rich olivine with ~10% Fe^{2+} in the divalent metal sites. As such most studies have focused on olivines of this composition. Natural forsterite also commonly contains trace quantities of Mn, Ni, Ca, and P. Microbes may be attracted to forsterite surfaces to harvest these trace elements and/or iron (e.g. Oelkers et al., 2015).

2.1. Forsterite solubility and dissolution rates as a function of chemical affinity

Critical to understanding the reactivity of a mineral is to have detailed knowledge of its solubility and its stability relative to other mineral phases. The concentration of magnesium in equilibrium with amorphous SiO_2, pure forsterite, and other Mg-silicate phases at 25 °C is shown in Fig. 2 as a function of pH. These and other thermodynamic calculations in this report have been made using the PHREEQC computer code together with its llnl database (Parkhurst and Appelo, 2013). The ambient temperature solubility of forsterite is extremely high at neutral to acidic pH. Even in the absence of complexing ligands, the concentration of Mg in equilibrium with forsterite and amorphous Si, which sets a practical limit for aqueous Si concentrations in > 100 °C experiments and in nature, exceeds 1 mol/kg at all pH < 7.9 at 25 °C. Moreover, the hydrous Mg-silicates sepiolite and crystolite are far less soluble than forsterite. As such, forsterite precipitation does not occur, and near to equilibrium conditions are difficult to attain at ambient temperatures. Consequently, most work on olivine surface reactivity to date has focused on its far-from-equilibrium dissolution kinetics.

As forsterite dissolution occurs at ambient temperatures in strongly undersaturated conditions, the interpretation of its dissolution rates is simplified. The overall dissolution rate of a mineral can be considered to be the difference between the forward rate (pure dissolution, r_+) and the reverse rate (precipitation, r_-) such that

$$r = r_+ - r_- = r_+\left(1 - \frac{r_-}{r_+}\right) \tag{1}$$

Taking account of the law of detailed balancing, it can be shown that Eq. (1) is equivalent to (Aagaard and Helgeson, 1977, 1982; Lasaga, 1981; Schott and Oelkers, 1995)

$$r = r_+(1 - \exp(-A/\sigma RT) \tag{2}$$

where σ stands for Temkin's average stoichiometric number equal to the ratio of the rate of destruction of the activated or precursor complex relative to the overall dissolution rate, A denote the chemical affinity of the reaction, T defines the absolute temperature, and R signifies the gas constant. The form of Eq. (2) is such that overall rates (r) equal forward rates (r_+) when $A \gg \sigma RT$. Due to its high solubility, most of the olivine dissolution rates reported in the literature have been measured at far-

[1] From this part of the manuscript onwards, the term forsterite will be used to identify forsteritic olivine having ~90% of Mg in its divalent metal site. The term 'pure forsterite' will identify the olivine comprised of 100% Mg in its divalent metal site.

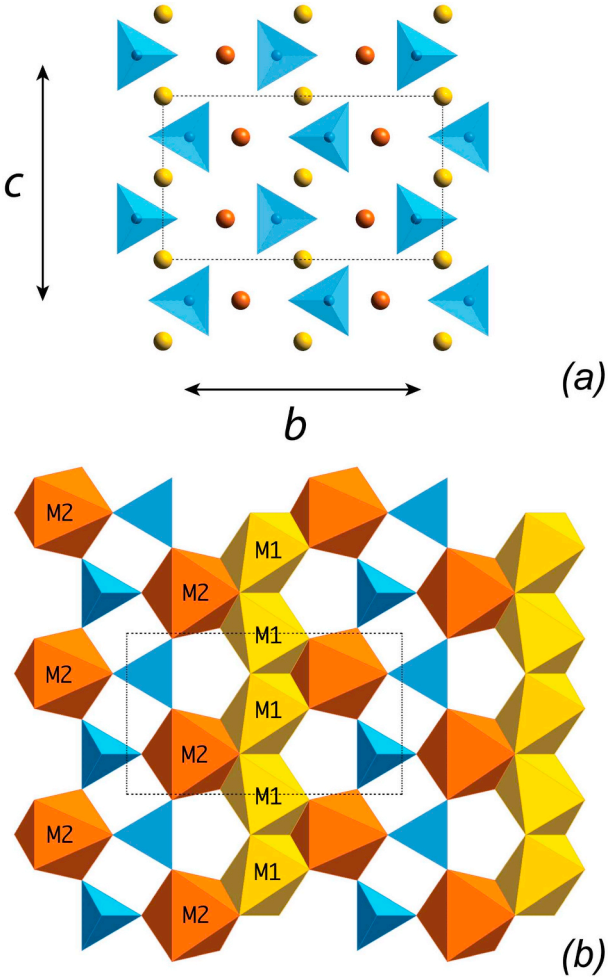

Fig. 1. Projections of the of olivine (Me_2SiO_4) structure down the *a* axis of the orthorhombic unit cell (dashed line). (a) Arrangement of two levels of the isolated SiO_4 tetrahedra aligned along the *b* and *c* axes and pointing alternately up and down along *c*; M1 and M2 cations are represented by yellow and orange colors, respectively. (b) Geometric distribution and connection of M1 and M2 octahedra relative to the SiO_4 tetrahedra on a single level of the unit cell.

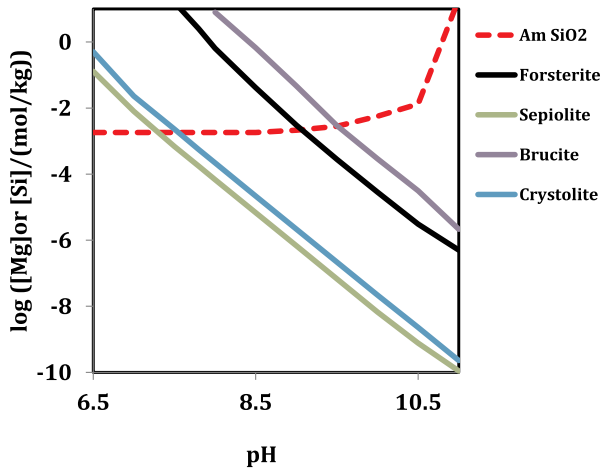

Fig. 2. Calculated variation with pH and a temperature of 25 °C of aqueous Mg concentrations in equilibrium with forsterite and amorphous SiO_2 Also included in this plot are the calculated aqueous SiO_2 concentrations in equilibrium with amorphous SiO_2. Concentrations shown in this figure were calculated using the PHREEQC computer code together with its llnl database – see text.

from-equilibrium conditions, such that $A \gg \sigma RT$. At these conditions $r_- \ll r_+$ and thus $r \approx r_+$. Consequently, measured ambient temperature forsterite dissolution rates can be used to assess the effect of aqueous solution composition and other factors on its forward dissolution rates independently from the effects of chemical affinity (e.g. the slowing of reaction rates as the system approaches equilibrium). The forward dissolution rate of the mineral, r_+, depends on the dissolution mechanism of the mineral. Insight, into the dissolution mechanism of forsterite, and other olivines can thus be gained by consideration of the variation of published rates as a function of aqueous fluid composition (see Section 3.1 below).

2.2. Forsterite dissolution mechanism

The dissolution mechanism of natural silicate minerals into aqueous solution depend on a large extent on the connectivity of its silica framework and the identity of the metal-oxygen bonds present in the structure of the mineral (e.g. Oelkers, 2001a; Brantley, 2008; Schott et al., 2009). As emphasized above, the forsterite structure consists of individual silicon–oxygen tetrahedra linked by magnesium atoms. As such olivine dissolution can proceed by the breaking of just the ionic Mg—O bonds, liberating the SiO_4^{4-} anions directly into solution. Due to both the absence of covalent Si—O—Si bonds and the relative weakness of the ionic divalent metal-oxygen bonds in its structure, olivine is among the fastest dissolving silicate minerals (e.g. Velbel, 1999).

The dissolution behavior of olivine, therefore, contrasts to that of most other multi-oxide minerals that require the breaking of more than one type of metal-oxygen bond. In such cases, the dissolution mechanism will consists of the sequential breaking of the bonds in the order of their reactivity typically via proton[2] for metal exchange reactions (e.g. Oelkers, 2001a). Consequently, the olivine dissolution mechanism is somewhat unrepresentative of that of most multi-oxide silicate minerals, but its simplicity allows insights into the dissolution mechanisms of these other minerals – see below.

Consistent with the observation that the ionic divalent metal-oxygen bonds break more rapidly than the covalent Si—O bonds, some of the earliest studies of forsterite-rich olivine dissolution reported an early rapid reversible exchange of Mg for protons on the olivine surface (Luce et al., 1972; Blum and Lasaga, 1988). This exchange was reported to be complete within a few minutes (Luce et al., 1972). The incorporation of protons by these reactions stems from 1) the need to maintain charge balance, and 2) the small size of protons, which allow these to be readily accommodated in the structure of the dissolving mineral. Further evidence for divalent metal for proton exchange reactions has been observed at acid conditions by XPS for the cases of forsterite (Pokrovsky and Schott, 2000a), fayalite (Fe_2SiO_4; Schott and Berner, 1983, 1985) and tephroite (Mn_2SiO_4; Casey et al., 1993a). The preferential departure of M^{2+} cations from this structure at acidic to neutral conditions is also consistent with the results of ab-initio quantum mechanical calculations reported by Liu et al. (2006). Blum and Lasaga (1988) and Wogelius and Walther (1991) found that natural San Carlos olivine surfaces consume as much as 10^{-5} to 10^{-4} mol/m^2 of protons during surface titrations. Oelkers et al. (2009), based on measured pH and the mass of Mg, Si and Fe released to aqueous solution during 20 min titrations, reported that on average 3.84 ± 0.59 protons were incorporated into the olivine structure for each Mg^{2+} removed from forsterite during surface titrations. This observation suggests that not only do the protons provide charge balance during this exchange reaction, but also charge the liberated Si—O bonds. Nevertheless, Casey (1991) and Westrich et al. (1993) using ion beam analysis determined that H^+ penetration into the olivine lattice is limited to depths of no > 100 nm, even for forsterite leached in pH 2 solutions. This

[2] The term proton in this manuscript is synonymous with the term hydrogen ion, which is present as hydronium ions in aqueous solution.

observation contrasts with their observation on several other silicate minerals, which show a deeper penetration of protons (e.g. Casey et al., 1988). The lack of significant H^+ penetration into the olivine structure likely stems from the fact that the SiO_4^{4-} tetrahedra are not interconnected. Once all the divalent metals surrounding a SiO_4^{4-} tetrahedra are replaced by protons, these tetrahedra are liberated and can pass into the aqueous phase so long as condensation (i.e. Si—O—Si dimerization) reactions do not occur at the surface. This contrast with the dissolution of chain-silicates like wollastonite, which is accompanied at acidic pH by H^+ penetration deep into the structure, promoting silica tetrahedral condensation leading to the formation of thick silica leached layers (Casey et al., 1993b; Schott et al., 2012).

The surface of freshly ground, but otherwise untreated, San Carlos olivine was studied in detail by Pokrovsky and Schott (2000a) and Oelkers et al. (2009). The isoelectric point, the pH at which suspended grains do not migrate under the influence of an electronic field, was determined to be 4.2 for San Carlos olivine in dilute aqueous NaCl solutions using zeta potential techniques. In contrast, traditional acid-base surface titrations of the surfaces of San Carlos olivine yield an apparent pH of zero point of charge equal to ~10. The large difference in these values was attributed to the exchange of protons for Mg immediately after fresh olivine surfaces are placed into the aqueous solution. As a result of this H for Mg exchange in the first one or two monolayers of the surface, the olivine surface exhibits an electrophoretic mobility similar to that of amorphous silica, which has an isoelectric point of 2.1. Also as a result of this Mg-for-H exchange, a Mg depleted layer, no > 20 Å thick was observed to form at the olivine surface at all pH < 9. A similar depletion of Mg from the surfaces of forsterite glass was observed at pH 4 by angstrom-scale resolved X-ray and FTIR data as reported by Morris and Wogelius (2008). At pH ~10 and higher, this exchange reactions reverses and a fine Si depleted Mg-rich layer is observed on forsterite surfaces. The excess release of Mg compared to that calculated from Si release and assuming stoichiometric dissolution from forsterite during short-term titrations is shown in Fig. 3. The observation that Mg is preferentially released at low to neutral pH but preferentially retained by the mineral structure in strongly basic solutions confirms the reversibility of the Mg for proton exchange reaction. The temporal variation of Mg versus Si release from dissolving forsterite at various pH was reported by Pokrovsky and Schott (2000b); the concentration of Mg and Si in reactive fluids recovered from two of their experiments are shown in Fig. 4. At pH 3, Mg is preferentially released for the first 40 min before stoichiometric dissolution was observed. In contrast, at pH 10, Si is preferentially released to the reactive fluid for the first ~100 h. The long time required to

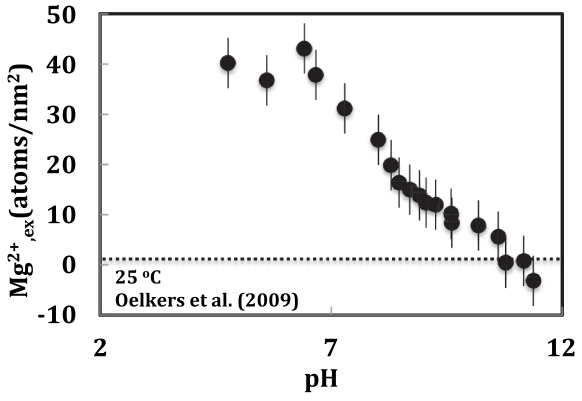

Fig. 3. Mass of Mg released from forsterite in excess of that calculated from Si release and the assumption of stoichiometric dissolution during 20 min batch titrations of the forsterite surface in units of atoms per nm^2 of forsterite surface (from Oelkers et al., 2009).

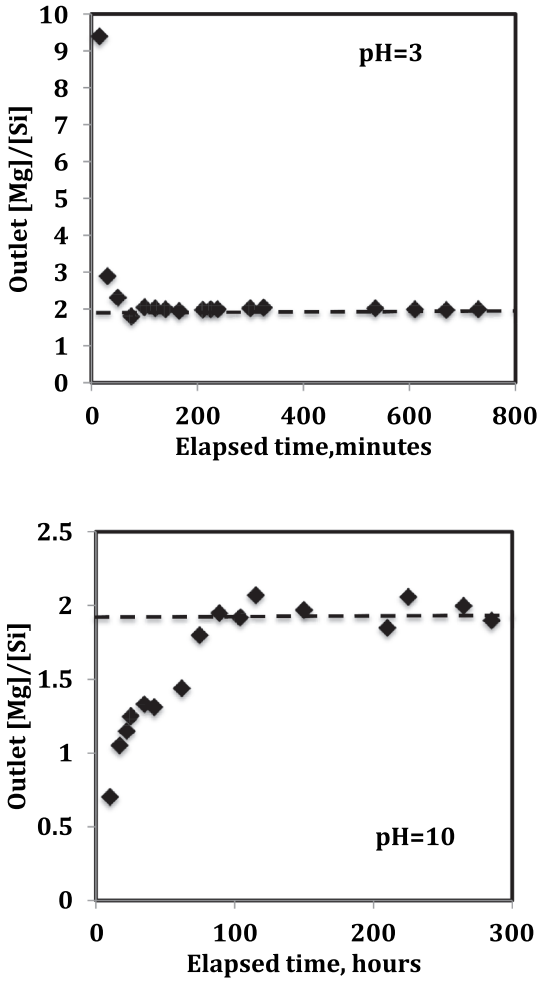

Fig. 4. Ratio of molar concentration of Mg to Si in the outlet fluids of forsterite mixed flow reactor dissolution experiments at pH 3 and 10 (after Pokrovsky and Schott, 2000b) – see text.

attain stoichiometric dissolution at basic pH could be attributable to the relative slow dissolution rates of forsterite at these conditions and the weak extent of its non-stoichiometric dissolution, which continues until the forsterite surface species (but not the bulk forsterite) has equilibrated with the reactive fluid. Taken together, this evidence shows that the early stages of olivine dissolution is non-stoichiometric due to the equilibration of its surfaces with the reactive fluid, and eventually stoichiometric after this surface has equilibrated.

The observations summarized above provide insight into how olivine dissolution proceeds. These observations include 1) olivine dissolution is limited by the breaking of its ionic octahedral M^{2+}-oxygen bonds, 2) these are the only bonds that need to be broken to dissolve the mineral and 3) its surface is M^{2+} poor at acid to mildly basic conditions but M^{2+} enriched at strongly basic conditions. Within transition state theory, the far from equilibrium dissolution rate of a mineral, r_+, is proportional to the concentration of its activated or precursor complex. Such complexes for minerals whose dissolution requires the breaking of only one type of cation–oxygen bond are formed by absorption reactions that tend to weaken this bond. Because the rate-controlling surface complexes for olivine dissolution are formed by adsorption reactions, olivine dissolution rates depend on the aqueous concentrations of those species that adsorb and weaken these bonds. The identity of such species will be reviewed below.

Table 1
Summary of experimentally measured forsterite steady-state dissolution rates studies reported in the literature.

Mineral	T, °C	Method	pH range	Notes	Reference
San Carlos Olivine (Fo92)	23–90	B	1–2	Rates measured as function of crystal orientation in H_2SO_4	Awad et al. (2000)
Balsam Gap Olivine (Fo93)	25	FB	1.8–11.35		Blum and Lasaga (1988)
San Carlos Olivine	65	B	2–5	Rates also measured as a function of aqueous Al^{3+} concentration	Chen and Brantley (2000)
San Carlos Olivine and pure Forsterite (Fo 100)	25	MF	1.95–11.85	Rates also measured as a function of aqueous CO_2 concentration	Golubev et al. (2005)
San Carlos Olivine	1–46	B	3–5	Assessed the effect of changing surface area during dissolution	Grandstaff (1978)
Hawaiian Beach Olivine	25	B	2		Grandstaff (1986)
San Carlos Olivine	90–150	MF	2–10.59	Rates also measured as a function of CO_2 and citric acid concentration	Hänchen et al. (2006)
Norwegian Olivine (Fo93)	60–90	B	−0.8 to 0.8	Experiments run in concentrated H_4SO_4	Jonckbloedt (1997)
Aimcor Olivine	25	B	0.6–6.5	Measured as in 0.2 m aqueous oxalate solutions	Liu et al. (2006)
Crestmore California Olivine (Fo91)	25	B	3.2–9.6		Luce et al. (1972)
San Carlos Olivine	25–65	MF	2	Rates also measured as a function of dissolved Mg and Si	Oelkers, (2001b)
Aimcor Olivine	25	B	1–4	Dissolved in concentrated $MgSO_4$, Na_2SO_4, $MgNO_3$ and HNO_3	Olsen et al. (2015)
Aimcor Olivine	25	B	0.6–6.5	Rates also measured as a function of aqueous oxalate concentration.	Olsen and Rimstidt (2008)
San Carlos Olivine	120	MF	3–8	Rates also measured as a function of CO_2, NaCl and $NaNO_3$ concentration	Prigiobbe et al. (2009)
San Carlos Olivine	25	MF	1.03–12.06	Rates also measured as a function of aqueous Mg, Si, and carbonate	Pokrovsky and Schott (2000a, 2000b)
Amicor Olivine	25–45	B	1.8–3.8		Rosso and Rimstidt (2000)
Dunite, North Carolina (Fo84)	25	B	4	Experiment run in dilute HNO_3	Siegel and Pfannkuch (1984)
Dreiser Weiher Olivine (Fo92)	40–70	B	1–3	Rates reported both in HCl and H_2SO_4	Van Herk et al. (1989)
San Carlos Olivine and pure Forsterite (Fo 100)	25–65	FB	1.8–12.4	Rates also measured as function of ascorbic acid, KH-phthalate and CO_2 concentration	Wogelius and Walther (1991)
San Carlos Olivine	65	FB	1.8–9.8	Rates also measured as a function of KH-phthalate concentration	Wogelius and Walther (1992)

B = Batch Reactor.
FB = Fluidized Bed.
MF = Mixed flow Rector.

3. Factors influencing olivine dissolution rates

3.1. Effect of surface area

It is commonly assumed that the overall reactivity of a mineral in water is proportional to its surface area. There is, however, considerable discussion over exactly which surface area should be considered in this regard. The simplest surface area that has been used to characterize mineral reactivity is the geometric surface area, which is the surface of a smooth geometric shape, such as a sphere or a cube of equal size to the mineral grains. A popular alternative is to use the surface area measured by inert gas adsorption techniques together with the Brunauer, Emmett and Teller (BET) approach (Brunauer et al., 1938). The advantage of this gas adsorption approach is that the size of the adsorbing gas (e.g. Kr or N_2) is similar to that of H_2O so is thought to be a good proxy for characterizing the interaction of a mineral surface with water. The ratio of the BET surface area to the geometric surface area is termed roughness factor, which is thus a measure of how different the true surface area is compared to that of a smooth geometric shape of the same size. Due to the lack of internal surface area in olivine (Brantley and Mellott, 2000) the determined roughness factors of olivines used in most experimental studies is low and typically ranges from 3 to 10. As such, regression of rate forsterite rate data to either the initial geometric or the initial BET surface area of grains used in dissolution experiments yield similarly accurate fits (Rimstidt et al., 2012).

The connection between BET surface area and mineral reactivity, however is likely complex. First, as noted in Section 3.4 below, the surface area normalized dissolution rate of a mineral can depend strongly on its crystallographic orientation (cf. Bandstra and Brantley, 2008; Daval et al., 2013; Pollet-Villard et al., 2016). This undermines the accuracy of using a single surface area to quantify the rates of a mineral grain consisting of numerous different crystallographic faces, in part as the relative proportion of each surface can change during the dissolution of the mineral. For example, Grandstaff (1978) observed that the BET surface area of crushed grains during laboratory experiments increased dramatically due to the formation of etch pits formed along lattice imperfections such as dislocations and cleavage planes. In their study the BET surface area of forsterite dissolved at pH 2.6 and 25 °C increased by a factor of 7 during its first 100 h of dissolution. Nevertheless, this increase in surface area was not accompanied by a concurrent and proportional increase in the dissolution rate of this forsterite. A similar behavior was found for quartz dissolution by Gautier et al. (2001), which was attributed by these authors to the fact that the surface area increase observed during etch pit formation consisted of relatively unreactive etch pit walls. Indeed, the formation of etch pits requires that the newly created etch-pit wall surfaces are far less reactive than the etch pit bottom to enable the growth of these dissolution features (see also Hövelmann et al., 2012; Luttge et al., 2013; Velbel, 2014). Although not explicitly stated, most experimental studies avoid these complications by normalizing rates to the initial surface area of the grains rather than the final surface area or the surface area of grains collected during the experiment. The challenges of defining the reactivity of complex minerals led Fischer et al. (2012) to argue that a more precise description of mineral dissolution rates could be obtained by considering mineral surfaces as a distribution of spatially varying rates rather than a single uniform rate averaged over the whole of the surface. No doubt such an approach would be closer to reality, but at present it is impractical due to our limited knowledge of the distribution of rates on mineral surfaces.

3.2. Surface area normalized forsterite dissolution rates obtained in the laboratory as a function of Mg, Si concentration, H_2O activity and pO_2

A large number of studies have focused on characterizing the dissolution rates of forsteritic olivine in aqueous fluids containing only forsterite components: Mg, Fe, Si, and simple inorganic acids and bases. A list of many of these studies is provided in Table 1. Forsterite dissolution rates were reported to be independent of dissolved Mg and Si concentration up to 1.4×10^{-3} and 7×10^{-4} mol/kg, respectively at 25 °C and pH ~2 by Oelkers (2001a). As suggested above, this observation was attributed to the fact that there are no Si−O−Si linkages in its structure, such that the breaking of Mg−O bonds is the only step

in the steady-state dissolution mechanism. Similarly Pokrovsky and Schott (2000b) and Rosso and Rimstidt (2000) reported that low concentrations of aqueous Mg had little effect on forsterite dissolution rates. This conclusion was confirmed and expanded upon by Olsen et al. (2015) who reported that there was little effect of aqueous Mg concentration on forsterite dissolution rates at concentrations as high as 4 mol/kg. Conversely, Daval et al. (2011) reported that forsterite dissolution rates in solutions containing aqueous Si concentrations approaching equilibrium with amorphous SiO_2 slowed due to the formation of a thin amorphous SiO_2 layer at the olivine surface– see Section 3.7 below. The lack of an effect of Mg and Si on rates in the absence of a SiO_2-rich layer at the mineral surface is consistent with the conclusions made above that only a single metal-oxygen bond needs to be broken to dissolve the forsterite structure. Moreover, as aqueous Mg and SiO_2 do not affect forsterite dissolution rates in the absence of the formation of theses layers, the increase in concentration of their aqueous species in the reactive aqueous fluid during forsterite batch dissolution experiments will not alter forsterite dissolution rates. As such, Mg and SiO_2 would be expected to be released from forsterite at a constant rate in the absence of secondary mineral formation in batch experiments, following an initial non-stoichiometric release due to the equilibration of the forsterite near-surface with the aqueous phase (see above). In these instances, the Mg and SiO_2 concentrations should increase linearly with time in batch reactors having a constant reactive fluid volume. This relatively simple behavior, which contrasts with many other silicates that have more complex far-from-equilibrium dissolution behavior, enables rates obtained from batch reactors to be consistent with those obtained from mixed flow reactors.

As is the case with aqueous Mg and SiO_2, Sugimori et al. (2012) observed that changing the partial pressure of oxygen did not alter forsterite dissolution rates significantly at temperatures from 15 to 55 °C and pH from 4 to 6.0. These authors did report, however, that the overall Fe release rate from forsterite decreased with increasing pO_2 due to the formation of Fe(III) hydroxide secondary phases in their reactors.

In contrast to the role of Mg and Si, a significant effect on forsterite dissolution rates was found when varying the activity of H_2O. In a regression of results from highly saline aqueous solutions of $MgSO_4$, Na_2SO_4, $Mg(NO_3)_2$ and KNO_3, Olsen et al. (2015) reported that forsterite dissolution rates at 25 °C and pH ranging from 2 to 4 are proportional to the activity of H_2O to the 3.26 ± 0.65 power. The role of water in the dissolution mechanism has been attributed to its involvement in releasing silica tetrahedra from the structure during the rate-limiting step of dissolution (Liu et al., 2006). Nevertheless, as the activity of H_2O is close to unity in most natural fluids, the variation of forsteritic olivine dissolution rates at given temperature and in simple fluid-mineral systems that do not contain substantial inhibiting substances or secondary minerals can be described using a simple function of pH. The only exception may be in environments with low water activities such as partially saturated soils or high ionic strength evaporate fluids.

3.3. Surface area normalized forsterite dissolution rates as a function of pH at ambient temperature

Forsterite dissolution rates reported in the literature as a function of pH in aqueous solutions containing only Mg, Si, Fe, and simple inorganic acids or bases are depicted in Fig. 5. Note the general consistency of the rates reported in most of the published studies other than two notable exceptions. The first exception is the data of Grandstaff (1978, 1986), which are approximately two orders of magnitude lower than the corresponding values reported in more recent studies. Both Murphy and Helgeson (1989) and Rimstidt et al. (2012) suggested that the surface roughness reported in the Grandstaff (1986) study was unusually high such that either their BET surface areas were incorrect or their grains had not been properly cleaned prior to the experiment. The second noteworthy exception is that the rates at basic pH conditions reported by Blum and Lasaga (1988) are significantly higher than the more recently published rates. These rates were based on Si release from olivine. As noted by Pokrovsky and Schott (2000b), Si is preferentially released from forsterite at basic pH, and stoichiometric Mg to Si release are only attained after several hundred hours after the

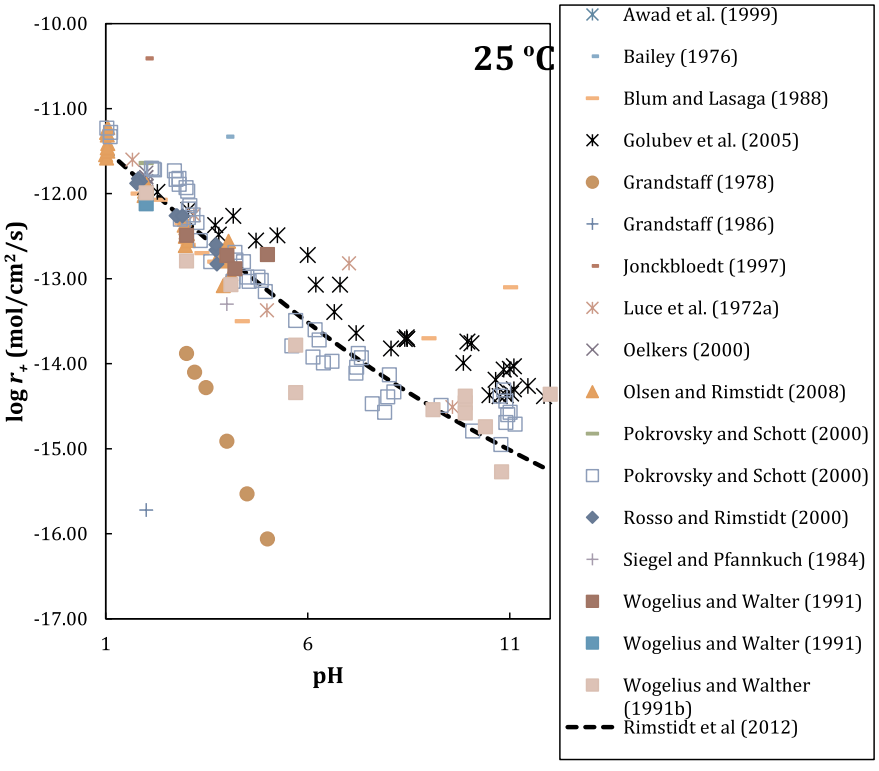

Fig. 5. Summary of experimentally measured forsterite steady-state dissolution rates reported in the literature at 25 °C as a function of pH. The symbols correspond to measured rates reported in the literature, whereas the curve was calculated using equations reported by Rimstidt et al. (2012). Note the data of Golubev et al. (2005), which are somewhat higher than other corresponding rates were obtained using pure synthetic Mg_2SiO_4 forsterite in contrast to the other illustrated data, which were obtained using forsterite containing up to 10% Fe its divalent metal sites – see text.

beginning of a dissolution experiment – see Fig. 5. This preferential early release of Si may likely be the origin of the anomalous fast forsterite dissolution rates at the basic pH conditions published by Blum and Lasaga (1988).

There are several noteworthy observations evident in Fig. 5. First, the consistency in reported rates at any pH is coherent with the conclusion that these rates are independent of aqueous Mg and SiO_2 concentrations. Second, forsterite dissolution rates appear to decrease monotonically with increasing pH. This behavior, which is common for the Mg-silicates (e.g. Oelkers and Schott, 2001; Saldi et al., 2007), contrasts with that of the aluminum bearing silicates, which tend to increase with increasing pH at basic conditions (e.g. Chou and Wollast, 1985; Gislason and Oelkers, 2003). This difference leads to distinct reactivities of these mineral groups. For example, the weathering of crystalline basalts is dominated by Mg-silicate dissolution at acidic conditions, but of Al-bearing silicates at basic conditions (Gudbrandsson et al., 2011). This leads to the preferential release of Mg and Fe from crystalline basalts at acidic conditions where dissolution is dominated by forsterite and pyroxene, but of Ca at more basic conditions where dissolution is dominated by plagioclase. The relative slow weathering rates of olivine compared to Al-silicate glass has been regularly observed in natural basaltic environments, where the fluid phase typically has a basic pH (Wasklewicz et al., 1993; Hausrath et al., 2008).

The apparent simple variation of forsterite dissolution rates with pH has led several investigators to fit these data to a pH function. Assuming forsterite dissolution can be described by two parallel reactions, one that dominates at acidic conditions and the other at basic conditions leads to (e.g. Rosso and Rimstidt, 2000; Marini, 2006; Palandri and Kharaka, 2004; Crundwell, 2014).

$$r_+ = r_a + r_b \tag{3}$$

where r_a and r_b refer to rates following the mechanisms that dominate at acidic and basic conditions, respectively. In each case, these rates are assumed to be dependent of the activity of H^+ in the aqueous solution in accord with the empirical relations

$$r_a = k_a a_{H^+}^{n_a} \tag{4a}$$

and

$$r_b = k_b a_{H^+}^{n_b} \tag{4b}$$

where k_a and k_b refer to rate constants, a_{H^+} designates the activity of aqueous H^+, and n_a and n_b represent reaction orders. There is a general consensus that the best reaction order at acid conditions is $n_a \sim 0.5$ (Rosso and Rimstidt, 2000; Marini, 2006; Palandri and Kharaka, 2004; Crundwell, 2014). Crundwell (2014) surveyed the reaction orders for forsterite dissolution in acidic solutions and reported that six studies containing 520 data points indicated a reaction order between 0.46 and 0.54. He argued that the reaction order of 0.5 is consistent with one H^+ ion forming an activated complex with a silica group at the forsterite surface and that water molecules react with the magnesium on these surfaces.

There are some differences in the literature, however, concerning the value of the reaction order at basic pH. The earlier studies, both in response to the rates available at that time and in an attempt to explain the dissolution behavior of all silicate minerals using the same approach, suggested that n_b should be negative with a value of -0.3 (Blum and Lasaga, 1988; Brady and Walther, 1989). More recent studies, however, have concluded that the rates at basic pH are most consistent with a slowly decreasing forsterite dissolution rate at basic pH. Rimstidt et al. (2012) proposed that n_b should be $+0.22$ and Crundwell (2014) proposed that n_b should be $+0.25$.

A summary of parameters derived to describe the BET surface area normalized forsterite dissolution rates as a function of pH are provided in Table 2, and compared in Fig. 6. It can be seen that the recent fits of 25 °C forsterite dissolution rate data yield nearly identical results as a function of pH, reflecting in part the consistency in the measured dissolution rates reported in the literature. The ability of these pH functions to describe the 25 °C forsterite dissolution rate data can be assessed by comparing the curve and data points in Figs. 5 and 6.

Table 2
Summary of rate parameters used in Eqs. (3) and (4a), (4b) to estimate BET surface area normalized forsterite dissolution rates as a function of pH at 25 °C.

	$\log k_a$	n_a	$\log k_b$	n_b
Wogelius and Walther (1991)	−11.04	−0.54	−16.63	0.31
Palandri and Kharaka (2004)	−10.85	−0.47	−14.64	0
Rimstidt et al. (2012)	−11.16	−0.44	−12.32	−0.22
Crundwell (2014)	−10.70	−0.5	−12.22	−0.25

An alternative approach to describe olivine dissolution kinetics is based on surface complexation models. After a relatively rapid equilibration over time frames of seconds to hours, the liable material at the olivine near surface equilibrates with its co-existing aqueous fluid phase. The equilibrated olivine surface has a unique composition at each pH, which can be described as consisting of distinct surface species. As such it seems reasonable to relate the dissolution rates to the concentration of these surface species. An early model, proposed by Blum and Lasaga (1988) suggested that forsterite dissolution rates are proportional to the concentrations of surface protonated sites at acidic conditions, and of deprotonated sites at basic conditions. A similar approach was adopted by Pokrovsky and Schott (2000a) who proposed a surface speciation model to describe olivine dissolution rates. These authors suggested that at acidic conditions forsterite dissolution is controlled by the decomposition of a silica-rich/magnesium-deficient protonated precursor complex. This complex was formed by the exchange of two hydrogens for a Mg atom leading to the condensation of two silica surface sites. This was followed by the adsorption of one proton onto the bridging oxygen of this dimer. In alkaline solutions, dissolution is assumed to be controlled by the decomposition of Mg hydrated sites in a Mg-rich layer formed by initial preferential silica release. Within this model, forsterite dissolution rates can be described assuming two parallel reactions occurring at silica-rich and hydrated Mg surface sites such that:

$$r_+ = k_{Si}\{>Si_2O\text{-}H^+\} + k_{Mg}\{>MgOH_2^+\} \tag{5}$$

where k_{Si} and k_{Mg} designate rate constants, and $\{>Si_2O\text{-}H^+\}$ and

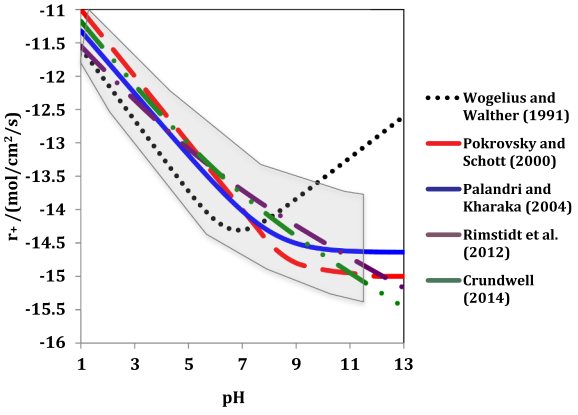

Fig. 6. Comparison of published forsterite dissolution rate equations as a function of pH at 25 °C. The equations used to compute each curve were reported by the references shown in the figure. The grey shaded region provides the approximate limits of the corresponding experimental data, other than those of Grandstaff (1978, 1986) and of Blum and Lasaga (1988) – see text and Fig. 5.

{ > $MgOH_2^+$} stands for concentration of the > $Si_2O\text{-}H^+$ and > $MgOH_2^+$ surface species, respectively. Although this model is not widely used owing to the challenges of calculating accurate surface speciation values, it can account for 1) for the reaction order of olivine dissolution rates with respect to H^+ activity at both acid and alkaline pHs, and 2) for the decrease in forsterite dissolution rates as a function of aqueous carbonate concentration at basic conditions, as the adsorption of this species onto forsterite surfaces decreases the concentration of the > $MgOH_2^+$ surface species. Rates computed with this model as a function of pH are compared with corresponding models in Fig. 6.

3.4. Effect of other dissolved inorganic species

3.4.1. CO_2

Because changing the aqueous concentration of CO_2 can lead to corresponding changes in aqueous solution pH, determining unambiguously the effect of CO_2 on mineral dissolution rates requires taking account of such pH changes. Prigiobbe et al. (2009) reported that there was no direct effect of changing the dissolved concentration of CO_2 on forsterite dissolution rates measured at 120 °C and pH 3 to 8. They concluded that any observed effects of increasing aqueous CO_2 on forsterite dissolution rates could be attributed to the changing of pH in the aqueous solution. Similarly, Golubev et al. (2005) observed no significant effect of the presence of 1 atm CO_2 on the dissolution rates of pure forsterite at 25 °C and pH ~4, nor of dissolved carbonate or bicarbonate at concentrations up to 0.009 and 0.005 mol/kg, respectively at pH from 8.45 to 11. In contrast, two studies reported a decrease of forsterite dissolution rates with increasing aqueous CO_2 concentration at basic pH (Wogelius and Walther, 1991; Pokrovsky and Schott, 2000b). This observation was attributed to the formation of a Mg-carbonate surface species lowering the concentration of the rate controlling hydrolyzed Mg surface species (see Section 3.3 above). The apparent inconsistency between these results and those of Golubev et al. (2005) could stem from the combination of different factors: the different duration of the experiments; the uncertainties in both pH and CO_3^{2-} activity in the studies; the possible influence of $Mg(OH)_2$ surface coatings, which might inhibit the dissolution reaction to some degree; and the fact that Golubev et al. (2005) used for most of their experiments a pure forsterite sample (Fo_{100}). Wogelius and Walther (1991), however, found that the dissolution rates of pure forsterite (Fo_{100}) were identical to that of a typical forsterite (Fo_{90}) at these conditions. As such, although the rapid rates of Fe oxidation at basic conditions might have led to the formation of a Fe(III) bearing secondary mineral at the olivine surface, it seems unlikely that such iron-rich coatings are inhibiting. It should also be noted that in both the Golubev et al. (2005) and Pokrovsky and Schott (2000b) studies the Mg and Si aqueous concentrations were close to detection limits and thus the source of large uncertainties.

3.4.2. Aqueous Al

Chen and Brantley (2000) reported that there was no effect of varying the concentration of aqueous Al from 0 to 10 ppm on forsterite dissolution rates at pH 2.95 and 65 °C.

3.4.3. Salinity

Prigiobbe et al. (2009) reported that there was no direct effect of changing the salinity, adjusted by changing aqueous NaCl and $NaNO_3$ concentrations over the range 0 to 2 mol/kg in the reactive fluid on measured forsterite dissolution rates at 120 °C and pH 3 to 8. A decrease in forsterite dissolution rates in more highly concentrated salt solutions was attributed to their effect on H_2O activity by Olsen et al. (2015) – see Section 3.2 above.

Taken together, there is little evidence that the changing of the aqueous concentrations of dissolved inorganic species effect directly forsterite dissolution rates other than perhaps with the exception of aqueous CO_2 at basic pH. The presence of such species can, however, alter forsterite dissolution rates indirectly through changes in pH or water activity.

3.5. Surface area normalized forsterite dissolution rates as a function of temperature

The variation of mineral dissolution rates as a function of temperature is almost exclusively described using some form of an Arrhenius equation. The application of the Arrhenius equation has, nevertheless, led to some confusion when applied to mineral dissolution rates. If derived from transition state theory, the Arrhenius equation suggests that the logarithm of the rate constant, k, equating the rate to the concentration of the rate controlling activated complex should be approximately a linear function of reciprocal temperature in accord with (cf. Schott et al., 2009).

$$k = A_o e^{-E_a/RT} \tag{6}$$

where A_o refers to a temperature independent pre-exponential factor, and E_a stands for the activation energy. Note that the rate constant is related to r_+, the forward dissolution rate, by

$$r_+ = kK\prod_i a_i^{n_i} \tag{7}$$

where K refers to the equilibrium constant for the reaction creating the activated or precursor complex and n_i denotes the stoichiometric number of moles of the ith species in the reaction creating 1 mol of this activated or precursor complex. Confusion arises as many have applied a form of the Arrhenius equation to describe the temperature dependence of reaction rates such as

$$r = A'_o\, e^{-E'a/RT} \tag{8}$$

where A'_o refers to a temperature independent pre-exponential factor, but E'_a stands for an apparent activation energy (see Casey and Sposito, 1993). The difference between E_a and E'_a, therefore, is the temperature variation of the concentration of the activated or precursor species, for example, the temperature dependence of the concentrations of the > $Si_2O\text{-}H^+$ and/or the > $MgOH_2^+$ surface species in the Pokrovsky and Schott (2000b) model. This subtle difference is responsible in part for inconsistencies in activation energies for mineral reactions reported in the literature (cf. Oelkers and Schott, 1999). In cases where the concentrations of the activated or rate controlling species decrease rapidly with increasing temperature, negative apparent activation energies can be observed, for example for the case of carbonate mineral dissolution rates at acidic conditions (Pokrovsky et al., 2009; Schott et al., 2009).

In aqueous solutions containing only Mg, Si, and simple inorganic acids, and having an activity of H_2O close to one, forsterite dissolution rates depend on only pH. So long as the dissolution mechanism remains independent of temperature and the enthalpy of the activated complex formation reaction is approximately constant, the constant pH dissolution rates of forsterite might be expected to be consistent with Eq. (8) such that the logarithm of its dissolution rates plot as a linear function of reciprocal temperature. Such appears to be the case, as evident in Fig. 7. With few exceptions, the pH = 2 far from equilibrium rates shown in this figure are closely consistent with Eq. (8) over the temperature range of 25 to 150 °C.

Such observations, together with the observation that forsterite dissolution rates in these inorganic systems depend only on pH, the variation of forsterite dissolution rates may be described using Eqs. (3) and (4a), (4b) together with

$$k_a = A_{o,a} e^{-E_{a,a}/RT} \tag{9a}$$

and

$$k_b = A_{o,b} e^{-E_{a,b}/RT} \tag{9b}$$

where $A_{O,a}$ and $A_{O,b}$ refer to temperature independent pre-exponential

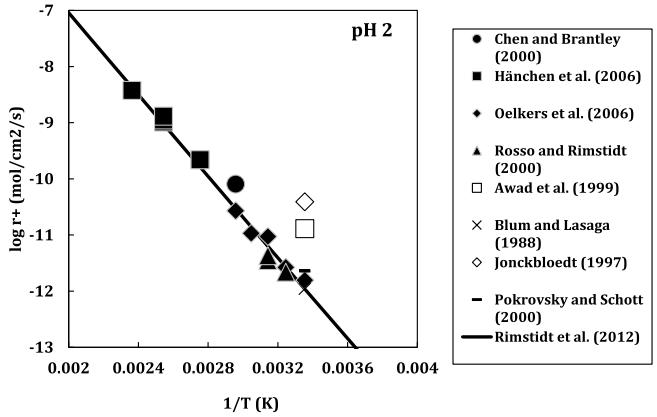

Fig. 7. Arrhenius plot of the pH 2 forsterite forward dissolution rates. The symbols correspond to measured rates reported in the literature, whereas the curve was calculated using equations reported by Rimstidt et al. (2012).

factors, and $E_{a,a}$ and $E_{a,b}$ stand for apparent activation energies. Note that if $E_{a,a}$ and $E_{a,b}$ are independent of temperature, the pH variation of forsterite dissolution rates at elevated temperatures will be similar to that at ambient temperatures.

A number of studies have reported forsterite dissolution rates at temperatures in excess of 25 °C (see Table 1). Chen and Brantley (2000) reported forsterite dissolution rates at 65 °C and 2 < pH < 5. After comparing their results with corresponding rates reported at 25 °C, these authors suggested that the pH variation of these rates varies with temperature and the apparent activation energy is pH dependent. From their analysis, they proposed that the activation energy for forsterite dissolution increased with pH from 84 to 125 kJ/mol as pH decreased from 5 to 0. A more comprehensive study performed by Hänchen et al. (2006) reported the dissolution rates of San Carlos forsterite determined at temperatures of 90, 120, and 150 °C and pH ranging from 2 to 12.5. In contrast to the earlier study of Chen and Brantley (2000) these authors found that forsterite dissolution rates exhibited a similar dependence on pH at each of these temperatures to that observed at 25 °C, and successfully fit their data, as well as literature data at 25 °C assuming a constant apparent activation energy of 52.9 ± 6.9 kJ/mol.

Taking account of these and other data, Rimstidt et al. (2012) fit a critically evaluated set of forsterite dissolution rates as a function of pH and temperatures from 25 to 150 °C using the combination of Eqs. (3), (4a), (4b) and (9a), (9b) consistent with

$$r_+ = A_{o,a} a_{H^+}^{n_a} e^{-E_{a,a}/RT} + A_{o,b} a_{H^+}^{n_b} e^{-E_{a,b}/RT}. \quad (10)$$

and the apparent activation energies of 70.4 and 60.9 kJ/mol at acidic and basic conditions, respectively. The consistency of their fit can be assessed with the aid of Figs. 7 and 8. The good fit of these data at temperatures from 20 to 150 °C and pH from 2 to 12 illustrate the simplicity of the variation of these rates as a function of temperature, and the ability of the Rimstidt et al. (2012) approach to describe these laboratory measured rates. These authors report that the error associated with rates calculated with this equation and the parameters listed in Table 2 are on the order of ~0.5 log units. It should be noted that Rimstidt et al. (2012) provided fits both based on geometric and BET surface area normalized rates; both providing equally good fits.

3.6. Effect of crystallographic orientation

Mineral dissolution occurs via the breaking of bonds. The breaking of bonds in the forsterite structure appears to be catalyzed by the adsorption of protons and/or water to these bonds. As each crystal face will have distinct compositions and bonding, it seems reasonable to expect that the rates of olivine dissolution will depend on the identity of each face. Such seems to be the case. Scanning electron microscope

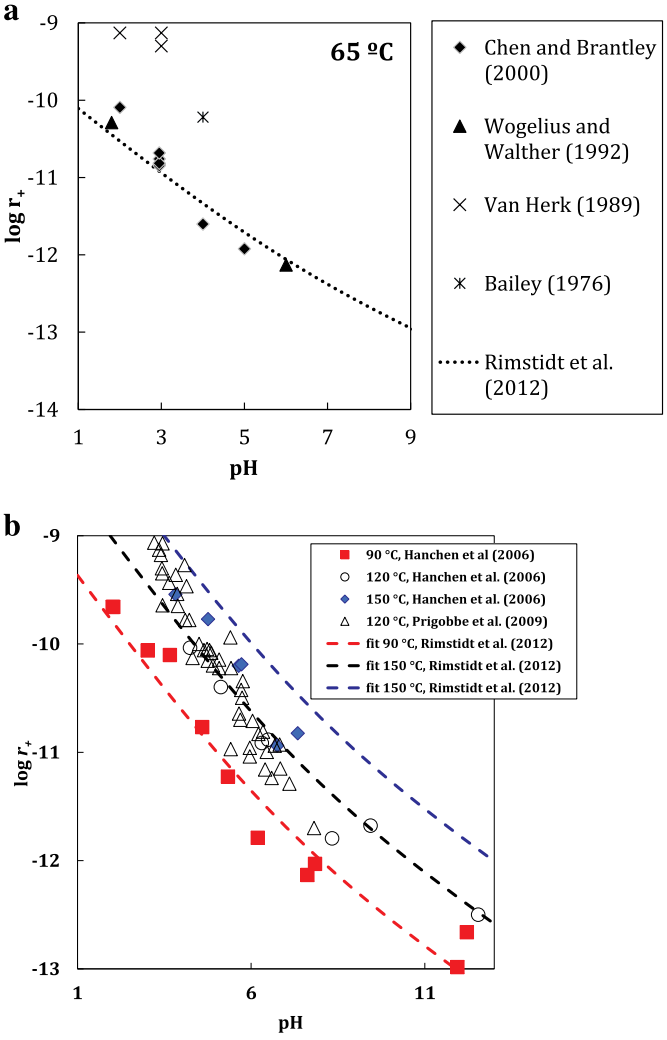

Fig. 8. Forsterite forward dissolution rates as a function of pH at a) 65 °C and b) 90, 120, and 150 °C. The symbols correspond to measured rates reported in the literature, whereas the curves were calculated using equations reported by Rimstidt et al. (2012).

images of forsterite grains reveal that some surfaces dissolve more rapidly than others, and that initial dissolution is enhanced along lattice imperfections such as dislocations and cleavage planes (Grandstaff, 1978). Awad et al. (2000) measured the dissolution rates of San Carlos olivine as a function of its crystallographic orientation in aqueous H_2SO_4 solutions and as a function of temperature. It was found that dissolution down the b-crystallographic axis at pH = 1 and 70 °C was on the order of 20 times faster than that down the a-axis. Olivine dissolution down the c-axis proceeded at a rate intermediate to those of the other axes. This observation was interpreted to stem from the enhanced protonation of oxygen atoms surrounding the M1 site of this olivine face. Note that such an interpretation is suspect as the M2 sites have longer metal-oxygen bond lengths, which would therefore tend to be more readily protonated. Other observations of heterogeneous reaction rates include those of King et al. (2014) who observed, using phase shift inferometry, that olivine dissolution rates vary from one surface to another, and can vary over the parts of the same crystallographic surfaces. They observed that the greatest surface retreat rates were associated with defects. Similar results were also found for willemite; Lin and Shen (1993) reported that the dissolution rates of distinct crystallographic planes of willemite differ by as much as a factor of 5 and the relative dissolution rates of these planes also varies with pH.

The effect of crystal orientation on rates is widely ignored as it is

common to measure dissolution rates on mineral powders. Such measurements will yield a surface area averaged dissolution rate. A justification for this approach is that mineral surfaces may be randomly distributed in natural systems. Surface area averaged rates may therefore make a good approximation to the rates found in natural systems. One consequence of heterogeneous rate distributions on mineral surfaces is that surface area normalized rates will tend to slow over time as a mineral dissolves. This results from the preferential dissolution of the more reactive parts of the surface leading to a less reactive surface over time. Such effects were detailed for the dissolution of clay minerals by Kohler et al. (2005). The surface area normalized dissolution rates of both forsterite and of quartz have been observed to decrease dramatically as these mineral dissolve during longer-term laboratory experiments (Grandstaff, 1978; Gautier et al., 2001).

3.7. The effect of amorphous SiO_2 and other mineral passivating layers

Various studies have found that the presence of secondary minerals or other mineral coatings can either slow considerably, or negligibly affect the dissolution rates of the underlying minerals. The mechanism for slowing the dissolution of a mineral through the formation of secondary mineral coatings requires the isolation of the original mineral surfaces from the reactive fluid. The degree to which secondary surface precipitates affect the dissolution rates of the primary mineral appears to depend on the structural match between the two minerals, the relative difference in solubility, and the presence of interconnected porous pathways in the secondary phases (Hodson, 2003; Cubillas et al., 2005; Putnis, 2009; Stockmann et al., 2011, 2013; Ruiz-Agudo et al., 2012; Saldi et al., 2013).

Several studies have shown that thin layers of amorphous Si can form on the olivine surface slowing its dissolution (e.g. Bearat et al., 2006; Jarvis et al., 2009; Daval et al., 2011; Wang and Giammar, 2012). Such fine surface layers can lower olivine dissolution rates by decreasing the surface area of the olivine directly exposed to the reactive fluid. The formation of amorphous SiO_2 layers is favored at low pH, where the olivine dissolution rate is elevated and the formation of secondary Mg-silicate minerals is unfavored by their high solubility (see Fig. 2). The formation of amorphous Si layers at these conditions is also favored by the Mg for proton exchange reaction, which creates an increasingly Si-rich surface as pH decreases at acidic conditions (cf. Pokrovsky and Schott, 2000b). Daval et al. (2011) detailed this effect, finding that forsterite dissolution rates approached zero as the activity of aqueous SiO_2 (a_{SiO_2}) approached equilibrium with amorphous SiO_2 (K_{SiO_2}, am) at 90 °C. Measured forsterite dissolution rates were found proportional to $a(_{SiO_2})/(K_{SiO_2}$, am), similar to the behavior observed for quartz (Berger et al., 1994; Gautier et al., 2001) and a number of multi-oxide silicate glasses (e.g. Grambow, 1985; Grambow and Muller, 2001; Daux et al., 1997; Gislason and Oelkers, 2003). A slowing of rates due to the formation of an amorphous SiO_2 coating at the forsterite surface was also reported by Johnson et al. (2014) at 60 °C. This latter study observed that while the presence of this layer slowed forsterite dissolution, it did not arrest dissolution, as the layer grew thicker on the surface. This suggests that the passivating properties of amorphous SiO_2 layers developed on the olivine surface may be *T*-dependent. The overall passivating or non-passivating properties of amorphous SiO_2 layers on olivine surfaces appears to depend on a competition between the rates of silicate hydrolysis and the rates of (re-)polymerization and densification of the constituting silica units. These processes influence the porosity of these layers, thereby controlling the inhibiting effect of the coating on the dissolution of the underlying phase (Cailleteau et al., 2008; Daval et al., 2011).

An important factor influencing the passivating effect of SiO_2 layers on olivine surfaces is the presence of ferric iron derived from the rapid oxidation of the Fe^{2+} released by the dissolving olivine. As reported by Saldi et al. (2013), the dissolution of pure forsterite (Fo100) under the same conditions tested by Daval et al. (2011) did not result in a significant decrease of olivine dissolution rates despite a copious precipitation of amorphous silica. The strong inhibiting effect of Fe-bearing SiO_2 layers was found to originate from the interaction of Fe(III) with SiO_2 under oxic conditions (Saldi et al., 2013, 2015; Sissmann et al., 2013). The incipient precipitation of hematite nanocrystals on the olivine surface, for example, can provoke adsorption and nucleation of amorphous SiO_2 from aqueous solutions that are undersaturated with respect to this solid, promoting its growth (Saldi et al., 2015). However, these authors showed that the degree to which such Fe-Si-rich layers isolate forsterite surfaces from dissolution depends on fluid redox conditions.

Although the effect of the presence of Fe^{3+} hydroxide mineral coatings on forsterite dissolution rates have not been directly studied, Golubev et al. (2005) compared the dissolution rates of pure forsterite and San Carlos olivine (Fo92) at pH ≥10. They found San Carlos olivine dissolution rates based on Mg release rate are approximately one order of magnitude slower than corresponding rates for pure forsterite. This slowing of olivine rates was attributed to the precipitation of Fe (III) hydroxide phases and/or Fe(II) in situ oxidation at the outermost edges of the olivine crystal surfaces as demonstrated in previous XPS analyses of olivine and fayalite grains reacted at pH ≥6 (Schott and Berner, 1983, 1985). These results are consistent with measurements of bronzite ($Mg_{1.777}Fe(II)_{0.227}Fe(III)_{0.011}Al_{0.013}Si_{1.98}$) dissolution rates at 25 °C and pH 6 which were found to be more one order of magnitude slower under oxic (pO_2 = 0.2 atm) than anoxic conditions (pO_2 = 0; Schott and Berner, 1983). These conclusions, however, are inconsistent with those of Wogelius and Walther (1991), who reported that the dissolution rates of pure forsterite (Fo_{100}) were identical to that of a typical forsterite (Fo_{90}) at basic pH.

Although there are far fewer studies of forsterite dissolution behavior at high pH, Golubev et al. (2005) noted that at 25 °C and pH > 10 forsterite dissolution was highly non-stoichiometric and suggested the formation of a $Mg(OH)_2$-like layer on the forsterite surface even in fluids that were undersaturated with respect to pure brucite. The degree to which the presence of such Mg-rich layers slows the dissolution rate of the original forsterite is currently unclear due to the lack of unambigious experimental observations. Stockmann et al. (2014) found that the formation of significant calcite precipitation on the surfaces of olivine at 25 °C and pH ~9 negligibly effected the dissolution rates of the underlying olivine. In these experiments, which lasted up to 7 months, the source material for the calcite coating the olivine was the injection of $CaCl_2$ and $NaHCO_3$ into the reactor, such that it was external to the dissolving olivine.

The observations summarized above suggest that the presence of secondary coatings on olivine surfaces can slow olivine dissolution. Evidence suggests that mineral/amorphous phases may strongly inhibiting olivine dissolution if either 1) the secondary phase has a close structural match with the dissolving olivine, and/or 2) the source material of the secondary phase originates from the olivine, as is the case with amorphous Si or $Fe(OH)_3$ coatings. In other cases there seems to be sufficient porosity and pathways in the coatings to allow the transport of aqueous phases to and from the bulk aqueous solution to allow forsterite dissolution to proceed relatively unaffected by the presence of these secondary coatings.

3.8. The effect of the presence of aqueous organic species

The effect of the presence of aqueous organic species in the reactive fluid on mineral dissolution rates can stem from either 1) the direct interaction of the organic species with the bonds that need to be broken to dissolve the mineral (e.g. Olsen, 2007; Olsen and Rimstidt, 2008), or 2) indirectly by changing the aqueous activity of elements that are either directly involved in the dissolution mechanism of the mineral (e.g. pH) or contribute to the chemical affinity (e.g. distance from equilibrium) of the fluid with respect to the dissolving mineral (e.g. Oelkers and Schott, 1998). For the case of olivine, as its dissolution rates are not

affected by the aqueous activity of metals in solution (e.g. Mg) and as its dissolution rates in laboratory studies have only been measured at far from equilibrium conditions, where rates are independent of chemical affinity, it seems likely that any influence of the presence of organic species on rates at constant pH would be attributed to the direct interaction of the species with the mineral surface.

The presence of dissolved aqueous organic species have been found to alter somewhat the dissolution rates of olivine (Grandstaff, 1986; Wogelius and Walther, 1991; Olsen and Rimstidt, 2008; Declercq et al., 2013). Grandstaff (1986) reported that forsterite dissolution rates were accelerated by up to two orders of magnitude at acidic conditions in the presence of either 0.1 mol/kg EDTA or 0.1 mol/kg potassium hydrogen phthalate (KHP), a commonly used aqueous organic pH buffer. Wogelius and Walther (1991) reported that San Carlos forsterite dissolution rates were accelerated by approximately 0.75 log units at pH 4 and in the presence of either 0.05 mol/kg aqueous KH-phthalate or 10^{-3} mol/kg aqueous ascorbic acid, but suggested this effect decreased with decreasing pH, as the presence of 0.05 mol/kg phthalic acid solution had little effect on forsterite dissolution rates at pH 2. Similarly, Hänchen et al. (2006) reported that 10^{-3} mol/kg citric acid increased forsterite dissolution rates at 90 °C by 0.25 log units at pH 3.4 and 0.5 log units at pH 4.5. This effect was attributed to the adsorption of these aqueous organics to surface Mg sites on the forsterite surface. Indeed the formation of phthalate–Mg chelate surface complexes at the surfaces of forsterite glass were observed by Morris and Wogelius (2008). Similarly Liu et al. (2006) showed the enhancement of olivine dissolution of approximately one order of magnitude in the presence of the presence of 0.02 M oxalic acid at all pH from 0 to 8. Olsen and Rimstidt (2008) extended this study somewhat measuring forsterite dissolution rates over the pH range 0 to 7 and up to 0.35 mol/kg aqueous oxalate. This latter study suggested that forsterite dissolution rates depend on both the concentration of oxalate and pH and proposed that this stems from the contribution to the rate of a reaction mechanism where the formation of the activated complex involved both a hydrogen and an oxalate ion to release H_4SiO_4 into solution. Similarly, forsterite carbonation experiments presented by Bonfils et al. (2012) suggested that the presence of aqueous citrate or EDTA had a strong accelerating effect on element release from dissolving forsterite in the presence of 20 bar CO_2 pressure at 120 °C. Declercq et al. (2013) reported that forsterite dissolution rates at 25 °C and pH 3 were altered by no > 0.2 log units by the presence of up to 0.1 mol/kg of 13 different aqueous organic ligands, including acetate, oxalate, citrate, $EDTA^{4-}$, glutamate, gluconate, malonate, aspartate, tartrate, malate, alginate, salycilate and humate. The relatively small effect of the presence of organic species on forsterite dissolution rates in this study might have been limited by the relatively low pH of the reactive fluids such that many of these organic ligands were mostly present at neutral aqueous organic acids. Torres et al. (2014) reported that the presence of deferoxamine, a siderophore that can be obtained from the soil bacteria *Streptomyces pilosus* can accelerate olivine dissolution by as much as an order of magnitude. As deferoxamine selectively binds Fe^{3+} rather than Fe^{2+}, Torres et al. (2014) postulated that the observed acceleration stemmed from this organic limiting the formation of iron (oxy)hydroxide secondary phases on the surfaces of the dissolving olivine; as mentioned above such secondary precipitates could limit the mineral-aqueous surface area slowing dissolution in the absence of this siderophore.

The above observations suggest that organic ligands can have a limited accelerating effect on the forsterite dissolution rates in acidic fluids. The limited effect of organic ligands at acidic conditions might be due to the lack of near surface Mg near the surface at these conditions (see Section 2.2). At neutral to basic conditions, Mg will be abundant at the forsterite surface and its removal could potentially be accelerated by absorbed organic ligands. At such conditions, the acceleration of forsterite dissolution rates by the presence of aqueous organic ligands has been found to be as much as two orders of magnitude for strongly chelating anions such as EDTA and phthalate.

3.9. The effect of the presence of microbial species

A significant number of studies have aimed to determine the effect of biomass on forsterite dissolution rates. Weber and Martinez (2017) reported that the presence of inactive Synechococcus cyanobacteria had no measurable effect on the dissolution rates of Aheim forsterite. In contrast to inactive bacteria, some studies have reported that active microbes lower substantially the dissolution rates of forsterite. Garcia et al. (2013) reported that the freshwater Proteobacterium *E. coli* inhibited significantly olivine dissolution. These authors attributed this inhibition to the coating of olivine surface by organic compounds decreasing the surface area of this mineral directly exposed to the reactive aqueous fluid. This conclusion concurs with that of Shirokova et al. (2012) who reported that the surfaces of forsterite in the presence of active aerobic gram-negative bacteria *Pseudomonas reactans* were rapidly covered in a biofilm-like material that decreased significantly the long-term dissolution rates at ambient CO_2 partial pressures. Similarly, Oelkers et al. (2015) determined that forsterite dissolution rates were slowed by an order of magnitude by the presence of *protobacteria* and fungi dominated by *Trichocomaceae*. Imaging of the mineral surfaces after this nearly 5 year-long experiment showed that the microbes selectively colonized the reactive sites present of the olivine surface limiting the overall dissolution rates. These authors suggested the selective colonization of these sites was due to the need of the microbes to harvest nutrients from the dissolving olivine.

Nevertheless there are some studies suggesting that microbial activity can enhance somewhat forsterite dissolution, likely indirectly through the changing of the composition of the aqueous fluid phase. Cai et al. (2013) reported that cultures of *Aspergillus niger* could accelerate forsterite dissolution somewhat by excreting oxalic acid to the aqueous fluid. Similarly, Shirokova et al. (2012) concluded that an observed increase in forsterite dissolution rates in the presence of dead and live *Psudomonas reactans*, an aerobic gram-negative bacteria, stemmed from the complexation of forsterite dissolution products by produced exudates and lysis products. Seiffert et al. (2014) suggested a minor increase in forsterite dissolution rates in the presence of the cyanobacterium *Nostoc punctiform* and the rock inhabiting ascomycete *Knufia peticola*. These authors attributed this increase to aqueous fluid pH changes induced by these species.

The dissolution behavior of fayalite in the presence and absence of *Acidithiobacillus ferroxidans* was studied at pH 2 using scanning electron and high-resolution electron microscopy by Welch and Banfield (2002). Similar to the effects of microbes on forsterite in many experiments, they observed a strong slowing of rates in the presence of *Acidithiobacillus ferroxidans*. These authors proposed that the slowing of rates was due to the adsorption of Fe^{3+} formed by the oxidation of the Fe^{2+} released to solution by the bacteria. In a similar set of experiments Santelli et al. (2001) reported that the presence of this bacteria lowered fayalite dissolution rates by 50 to 98% compared to corresponding abiotic experiments performed at pH ranging from 2 to 4.

3.10. Dissolution rates of non-forsteritic olivine and similar minerals as a function of temperature and mineral composition

Owing to their relative rarity, relatively few studies have characterized the dissolution rates of the non-forsteritic olivines and the similarly structured and compositioned phenacites. A summary of these studies is provided in Table 3. Among the most common of these is fayalite (Fe_2SiO_4), the iron end member of this mineral family. The study of fayalite dissolution kinetics is confounded by the oxidation of aqueous divalent iron at neutral to basic conditions. Fayalite dissolution kinetics were studied by Siever and Woodford (1979), Schott and Berner (1983, 1985), Siegel and Pfannkuch (1984), Wogelius and Walther (1992), and Westrich et al. (1993). Of these studies only Siever and Woodford (1979), Wogelius and Walther (1992), and Westrich et al. (1993) reported rates and only at pH 2 to 4.5 at 25 °C. In contrast,

Table 3
Summary of experimentally measured non-forseritic olivines and phenacites steady-state dissolution rates reported in the literature.

Mineral	Formula	pH	Temp, °C	Reference
Ca-olivine	Ca_2SiO_4	2.5–4.7	25	Westrich et al. (1993)
Co-olivine	Co_2SiO_4	1.9–6	25–45	Westrich et al. (1993)
Co-Mg-olivine	$Co_{1.45}Mg_{0.55}SiO_4$	2–6	25	Westrich et al. (1993)
Co-Mn-olivine	$Co_{1.1}Mn_{0.9}SiO_4$	2–7	25–45	Westrich et al. (1993)
Fayalite	Fe_2SiO_4	4.5	25	Siever and Woodford (1979)
Fayalite	Fe_2SiO_4	1–6	25	Schott and Berner (1983, 1985)
Fayalite	Fe_2SiO_4	N/R	22	Siegel and Pfannkuch (1984)
Fayalite (Fo6)	Fe_2SiO_4	2–4.5	25	Wogelius and Walther (1992)
Kirschsteinite	$CaFeSiO_4$	2–6	25	Westrich et al. (1993)
Liebenbergite	Ni_2SiO_4	1–3	25–70	Westrich et al. (1993)
Monticellite	$CaMgSiO_4$	2–9	25–45	Westrich et al. (1993)
Phenacite	Be_2SiO_4	1–3	25–50	Westrich et al. (1993)
Tephroite	Mn_2SiO_4	2–8	25–45	Casey et al. (1993a, 1993b)
Willemite	$ZnSiO_4$	0.31–3	31–94	Terry and Monhemius (1983)
Willemite	$ZnSiO_4$	1–4	30	Lin and Shen (1993)

Schott and Berner (1983, 1985) used XPS observations to characterize the reacted fayalite surfaces. These latter studies demonstrated a strong preferential release of Fe to solution relative to Si at pH 1.5 but the precipitation of a hydrous ferric oxide layer on fayalite surface at pH 6 under oxic conditions.

Westrich et al. (1993) also reported dissolution rates for a variety of other divalent metal olivines and phenacites at acidic to neutral pH and temperatures ranging from 25 to 70 °C. The dissolution rates of each of these minerals exhibit similar behaviors over the conditions studied. Each had dissolution rates that decreased by ~0.5 orders of magnitude with each pH unit increase in acid conditions, and each had an activation energy of 56 ± 6 kJ/mol. These behaviors are identical within uncertainty to those of forsterite but the magnitude of the rates are apparently related to the strength of the rate controlling M−O bonds in their structure. This observation is strongly consistent with the conclusion that the dissolution of all olivine and phenacite minerals proceeds via the breaking of these ionic divalent metal–oxygen bonds.

The 25 °C dissolution rates of several divalent metal olivines and phenacites are compared in Fig. 9. The corresponding dissolution rates of these minerals range over a span of approximately 6 orders of magnitude, with the Ca-olivine having a pH 2 dissolution rate of $10^{-8.5}$ mol/cm^2/s whereas the Be-bearing phenacite, has a rate of $10^{-14.7}$ mol/cm^2/s. This large range of rates for similarly structured silicates highlights the importance of the identity of the metal-oxygen bonds that need to be broken on the overall dissolution rate. It is instructive to note that the relative order and approximate value of breaking a metal oxygen bond appears to be similar in minerals of different structure. For example the 25 °C, pH = 2 dissolution rates of the divalent metal olivines and phenacites are plotted as a function of the corresponding dissolution rates of the divalent oxide minerals in Fig. 10. Although some scatter is apparent, as pointed out by Casey (1991), a strong positive correlation can be seen between the corresponding rates. As only a limited number of dissolution rates are available for metal oxide minerals, some have used the rates of water exchange on aqueous metals as a proxy for the oxide dissolution rates. For example, Casey and Westrich (1992) reported a strong correlation between the dissolution rates of the olivines and phenacites on one hand and the water exchange rates of the divalent metals on the other. A similar correlation between aqueous divalent metal-water exchange rates and metal carbonate mineral dissolution rates was reported by Pokrovsky and Schott (2002). In addition, quantum mechanical models suggest that the dissolution rates of the olivine series minerals are proportional to the length of the bond to their M sites (Liu et al., 2006).

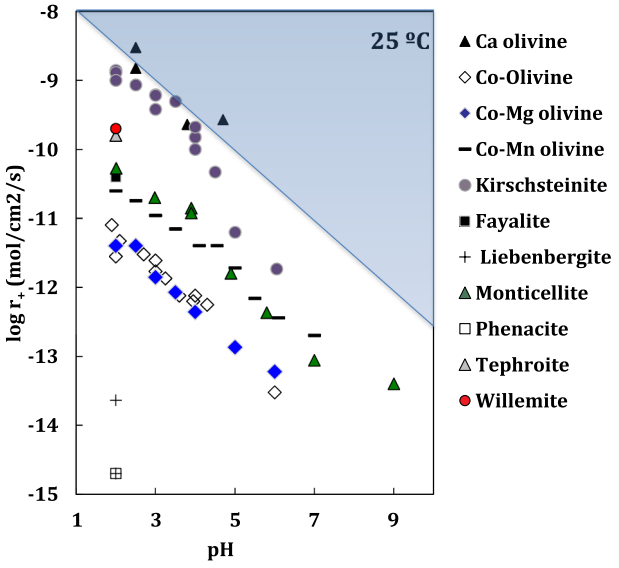

Fig. 9. Summary of experimentally measured non-forsteritic olivine steady-state dissolution rates reported in the literature at 25 °C as a function of pH. The sources of data are listed in Table 3. The dissolution rate of Co-olivine at pH 6, 25 °C, shown in the figure was taken from Fig. 4 of Westrich et al. (1993) rather than from their table in annex 1. The later value is inconsistent with the trend of the data and appears to be a typographical error. The slope of the blue light triangle is −0.5 consistent with a variation of rates on pH of $r_+ \propto a_{H^+}{}^{-0.5}$.

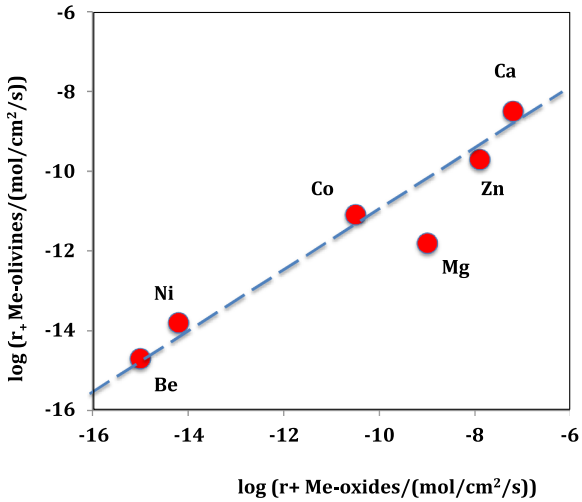

Fig. 10. The logarithm of divalent metal olivine dissolution rates as a function of the corresponding logarithm of divalent metal oxide dissolution rates at 25 °C and pH 2. Values for the olivines were taken from the references listed in Tables 1 and 3, whereas those of metal oxides were compiled by Casey (1991).

4. Applications

4.1. Forsterite and Mg isotope compositions of natural waters

The initial dissolution of forsteritic olivine leads to the preferential departure of isotopically light Mg (Maher et al., 2016). In their study, performed in batch reactors, Maher et al. (2016) found that over time the isotopic composition of the fluid phase becomes equivalent to the dissolving forsterite in the absence of secondary mineral precipitation. Similarly Wimpenny et al. (2010), observed a similar initial release of light Mg during the dissolution of forsterite at highly undersaturated conditions at basic pH followed by a return towards the conservative

release of Mg over time in mixed-flow reactors. Such a behavior can originate from the preferential breaking of ^{24}Mg—O bonds or from a distinct isotopic fractionation of Mg at the surface compared to that with the mineral structure.

More commonly, in natural systems, forsterite dissolution is accompanied by the formation of secondary minerals and biotic processes. A number of studies demonstrated that such processes may alter the Mg isotopic composition of residual fluids (e.g. Teng et al., 2007, 2010; Black et al., 2008; Bolou-Bi et al., 2010; Li et al., 2010; Wimpenny et al., 2010; Opfergelt et al., 2012, 2014; Pogge von Strandmann et al., 2008; Shirokova et al., 2013; Tipper et al., 2010; Huang et al., 2012; Ilina et al., 2013; Mavromatis et al., 2012, 2014; Prikryl et al., 2018). Tipper et al. (2006) argued that such processes could lead to global riverine fluxes that are isotopically lighter in Mg compared to the homogenous chondritic composition of the Earth's mantle. The degree to which lighter or heavier Mg is uptaken may depend on the mineral or processes consuming the Mg liberated by the dissolving forsterite. Oelkers et al. (2015) found that the isotope composition of Mg released to the fluid from dissolving olivine, covered in part with bacteria, dominated by *Rhizobiales* (*Alphaproteobacteria*), and fungi, dominated by *Trichocomaceae*, was 0.25‰ heavier in $\delta^{26}Mg$ than the dissolving forsterite. This study attributed the non-conservative release of Mg to the preferential uptake of light Mg by the microbial community. In the experiments reported by Wimpenny et al. (2010), forsterite was dissolved in controlled conditions at pH 10 and 11 at various fluid saturation states with respect to the dissolving forsterite but at close to equilibrium conditions with respect to chrysotile. The reactive aqueous fluid became enriched in heavy Mg, suggesting that this secondary phase preferentially consumed light Mg. Similarly, the formation of carbonate minerals is known to preferentially remove isotopically light Mg isotopes from aqueous solution (Tipper et al., 2006; Pearce et al., 2012; Mavromatis et al., 2014; Beinlich et al., 2014; Schott et al., 2016). This contrasts with the behavior of other secondary Mg-silicate minerals, which have been observed to preferentially uptake heavier Mg (e.g. Pogge von Strandmann et al., 2008). As such, the combined effect of forsterite dissolution, microbial activity, and secondary mineral precipitation can lead to the overall release of either relatively heavy or relatively light Mg depending on the identity and relative importance of the secondary minerals and the role of microbes.

4.2. Forsterite dissolution and carbon storage

Much recent work has been aimed at constraining the potential of enhanced weathering to attenuate the increase in atmospheric CO_2 concentrations (e.g. Schuiling and Krijgsman, 2006; Hangx and Spiers, 2009; Kohler et al., 2010, 2013; Hartmann et al., 2013; Moosdorf et al., 2014; Renforth et al., 2015; Griffioen, 2017; Montserrat et al., 2017; Weber and Martinez, 2017). The goal of enhanced weathering efforts is to apply finely grained reactive divalent metal-rich silicate minerals in the oceans or on soils to draw down CO_2 directly from the atmosphere. The dissolution of these minerals will increase fluid alkalinity and release Ca^{2+} and Mg^{2+} to the aqueous phase promoting the formation of carbonate minerals. Among the silicate minerals, forsterite is among the most considered due to its high reactivity and abundance (e.g. Oelkers et al., 2008a). The results summarized in this review, however, suggest that there are very few options to increase the rates of forsterite dissolution for enhanced weathering. The only processes that can substantially increase forsterite dissolution rates appear to be 1) increasing forsterite surface area, and/or 2) decreasing aqueous fluid pH. Although some organic ligands could enhance rates at neutral to basic conditions, it seems unlikely that these could be added in large quantities into soils or the ocean without substantial environmental consequences. Consequently, some have even considered extensive ball milling of this material to further accelerate the release of metals from this material (Haug et al., 2010; Rigopoulos et al., 2015, 2016).

The potential of forsterite to attenuate atmospheric CO_2 levels stems largely from the alkalinity generated as it dissolves. The stoichiometric dissolution of typical natural olivine, for example, according to the reaction

$$Mg_{1.8}Fe_{0.2}SiO_4 + 4H^+ = 1.8Mg^{2+} + 0.2Fe^{2+} + SiO_2 + 2H_2O \quad (11)$$

consumes four protons per mole of olivine. This reaction increases the pH and in turn increases the solubility of CO_2 in fresh and seawater through the reactions:

$$CO_{2(g)} + H_2O = H_2CO_{3(aq)}, \quad (12a)$$

$$H_2CO_{3(aq)} = H^+ + HCO_3^-, \quad (12b)$$

$$H_2CO_{3(aq)} = 2H^+ + CO_3^{2-}, \quad (12c)$$

which illustrate the increase of carbonate alkalinity (HCO_3^- and CO_3^{2-}) with increasing pH, while the concentration of dissolved aqueous CO_2 (e.g. $H_2CO_{3(aq)}$) is fixed by the partial pressure of atmospheric $CO_{2(g)}$ in accord with Eq. (12a). This process would lead to as much as 4 mol of CO_2 dissolved into water or seawater per mole of forsterite dissolved, as seawater is dominated by the HCO_3^- species. The efficiency of this process, unfortunately, decreases when secondary precipitates are formed. For example, the increase of pH in response to reaction (11) could provoke calcite precipitation in the ocean via

$$Ca^{2+} + 2HCO_3^- = CaCO_3\,(calcite) + CO_2(g) \quad (13)$$

where the dissolved calcium required for this reaction comes from that already dissolved in seawater. The liberation of CO_2 by this reaction reduces the efficiency of enhanced weathering by about a factor of two compared to that without secondary precipitation. Furthermore, the buildup of Mg, in part due to sluggish magnesite precipitation kinetics at ambient temperatures (Saldi et al., 2009, 2012) could provoke the formation of Mg clays such as sepiolite (c.f. Rigopoulos et al., 2018) in accord with

$$4Mg^{2+} + 6SiO_2 + 11H_2O = Mg_4Si_6O_{15}(OH)_2{\cdot}6H_2O + 8H^+ \quad (14)$$

which would further limit the efficiency of the enhanced weathering effort. The combination of secondary mineral precipitation limiting the efficiency of forsterite's ability to draw down CO_2 from the atmosphere, and the limited options available to accelerate forsterite dissolution rates poses a considerable challenge to making enhanced weathering of forsterite an efficient option for combating the current increasing atmospheric CO_2 levels.

Further efforts have explored the potential for carbonating olivine at elevated temperatures and/or in the subsurface (Giammar et al., 2005; Garcia et al., 2010; Xiong and Giammar, 2014; Xiong et al., 2017). Such efforts are motivated by the results of thermodynamic calculations such as for the reaction

$$\underset{(Forsterite)}{0.5\,Mg_2SiO_4} + CO_2 = \underset{(Magnesite)}{MgCO_3} + \underset{(Quartz)}{0.5\,SiO_2} \quad (15)$$

Calculated Gibbs Free energies of this reaction are plotted as a function of temperature for selected CO_2 partial pressures in Fig. 11a. The Gibbs Free energy of reaction (15) is negative, favoring the transformation of forsterite to magnesite only at temperatures of < 150 and 380 °C for a pCO_2 of 1 and 200 bars, respectively. The univarient curve showing the equilibrium temperatures and pCO_2 for this reaction are shown in Fig. 11b.

Critical to optimizing the forsterite carbonation process, however, is the observation that a large number of non-carbonate phases can potentially form from the interaction of forsterite with CO_2 rich-aqueous solutions. The stability fields of the most thermodynamically stable solids in the $MgO\text{-}SiO_2\text{-}H_2O\text{-}CO_2$ system are illustrated as a function of temperature and the partial pressure of CO_2 in equilibrium with the aqueous fluid (pCO_2) in Fig. 12. Forsterite is unstable at all temperatures and CO_2 partial pressure considered in this figure. In the absence of CO_2, forsterite is favored to react to form serpentine and brucite in

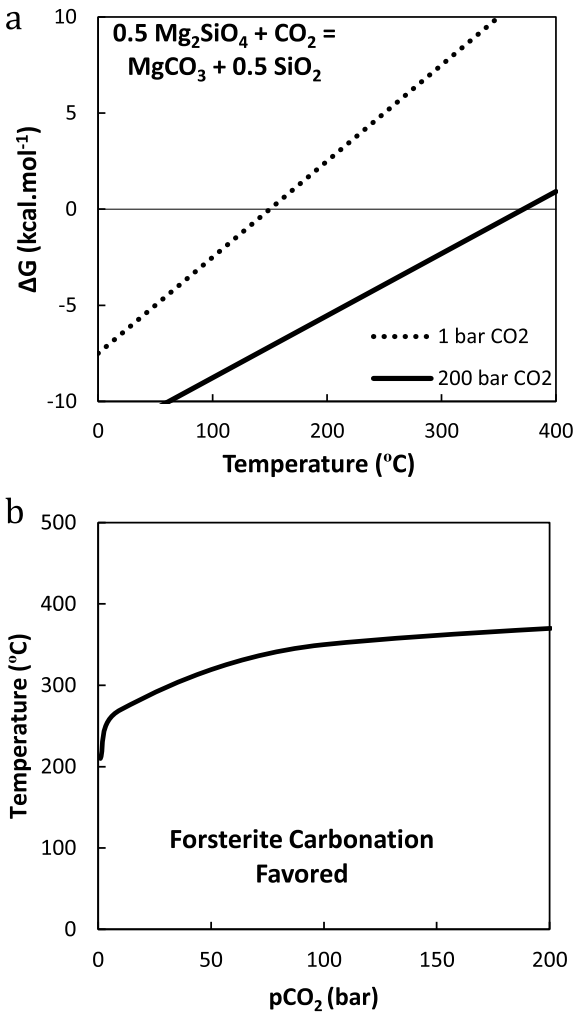

Fig. 11. a) Gibbs free energy of reaction (15) at 1 and 200 bars of CO_2 pressure as a function of temperature. The solid horizontal line corresponds to $\Delta G = 0$ for the reaction. b) Univarient curves showing the equilibrium temperature for reaction (15) as a function the partial pressure of CO_2.

accord with

$$\underset{\text{(Forsterite)}}{2Mg_2SiO_4} + \underset{\text{(Water)}}{3H_2O} = \underset{\text{(Serpentine)}}{Mg_3Si_2O_5(OH)_4} + \underset{\text{(Brucite)}}{Mg(OH)_2} \quad (16)$$

At $pCO_2 > 0.001$ bars at 120 °C and 0.046 bars at 200 °C the conversion of brucite to magnesite is favored. From these pCO_2 to 0.21 and 3.6 bars at 120 and 200 °C, respectively, forsterite is favored to convert to serpentine and magnesite in accord with

$$\underset{\text{(Forsterite)}}{Mg_2SiO_4} + CO_2 + \underset{\text{(Water)}}{2H_2O} = \underset{\text{(Serpentine)}}{Mg_3Si_2O_5(OH)_4} + \underset{\text{(Magnesite)}}{MgCO_3} \quad (17)$$

Although this reaction does carbonate forsterite, roughly 75% of the Mg released by forsterite dissolution is consumed by serpentine precipitation. From 0.21 bars $< pCO_2 <$ 1.7 bars at 120 °C, and from 3.6 bars $< pCO_2 <$ 33.9 bars at 200 °C, forsterite is favored to convert to talc and magnesite in accord with

$$\underset{\text{(Forsterite)}}{4Mg_2SiO_4} + 5CO_2 + \underset{\text{(Water)}}{H_2O} = \underset{\text{(Talc)}}{Mg_3Si_4O_{10}(OH)_2} + \underset{\text{(Magnesite)}}{5MgCO_3} \quad (18)$$

At these conditions roughly 37.5% of the Mg released by forsterite dissolution is consumed by talc precipitation. Only at higher pCO_2 the complete carbonation of the Mg contained in forsterite, consistent with reaction (15), is thermodynamically favored to occur. If for some reason quartz is kinetically inhibited to precipitate, the pCO_2 required to favor the complete carbonation of the Mg contained in forsterite as magnesite and amorphous Si is 21.4 and 223.8 bars at 120 and 200 °C, respectively. The distribution of the phase regions shown in Fig. 12 matches closely that previously calculated using thermodynamics databases and observed during the natural alteration of peridotite (Klien and Garrido, 2011). Note a lower temperature limit for the carbonation of forsterite added to Fig. 12 has been set to 75 °C, which is approximately the lowest temperature for which magnesite has been observed to precipitate from aqueous solution (Saldi et al., 2009, 2012; Case et al., 2011; Johnson et al., 2014). At lower temperatures magnesite precipitation appears to be kinetically inhibited. Note however that the formation of a mixture of nesquehonite ($MgCO_3 \cdot 3H_2O$) and magnesite has been observed in H_2O-saturated supercritical CO_2 at 35 and 50 °C

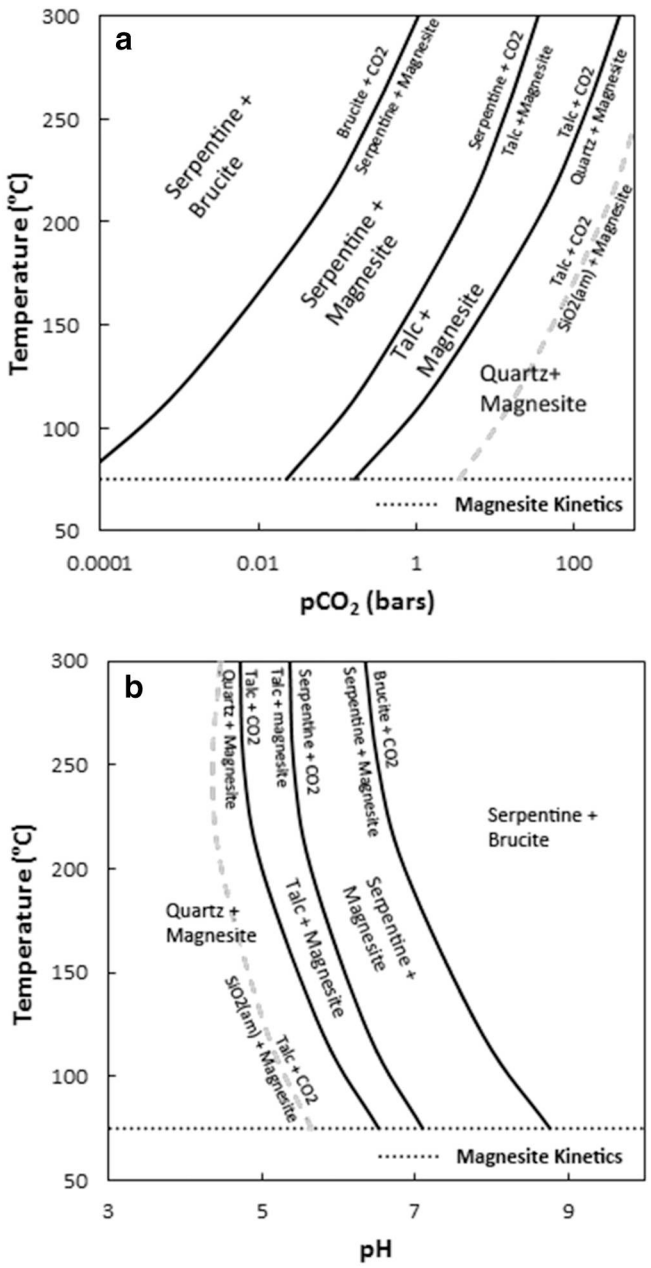

Fig. 12. a) Stability regions of minerals in the presence of H_2O in the system MgO-SiO_2-H_2O-CO_2 as a function of temperature and partial pressure of CO_2; b) pH of the univarient curves shown in Fig. 2a.

by Felmy et al. (2012). Moreover, at near ambient temperatures, nesquehonite (Hopkinson et al., 2012) and hydromagnesite ($Mg_5(CO_3)_4(OH)_2{\cdot}4H_2O$) formation (Gautier et al., 2014; Berninger et al., 2014) could contribute to the consumption of the Mg released by olivine dissolution. The pH corresponding to the equilibrium curves shown in Fig. 12a is shown in Fig. 12b. As one progresses to higher pCO_2 and the products of forsterite carbonation become increasingly magnesite rich, the pH of the system becomes increasingly acidic. Forsterite carbonation process is therefore may be more efficient at mildly acidic conditions rather than at basic conditions. Such results are also consistent with those of Snaebjornsdottir et al. (2018), who concluded that the most efficient carbonation of basalts occurs at relatively low pH conditions, where the precipitation of secondary divalent metal bearing silicate minerals is thermodynamically unfavored.

4.3. The generation of hydrogen and methane from olivine dissolution

A number of studies have postulated that it might be possible to generate either hydrogen or methane from the low temperature oxidation of Fe^{2+} released from olivine in accord with reactions such as (e.g. Hellevang et al., 2011; Etiope et al., 2013)

$$\underset{\text{Forsterite}}{Mg_{1.8}Fe_{0.2}SiO_4} + 1.36H_2O = \underset{\text{Serpentine}}{0.5Mg_3Si_2O_5(OH)_4} + \underset{\text{Brucite}}{0.3Mg(OH)_2} + \underset{\text{Magnetite}}{0.067Fe_3O_4} + 0.067H_2 \quad (19)$$

or

$$\underset{\text{Forsterite}}{Mg_{1.8}Fe_{0.2}SiO_4} + 1.9CO_2 + 0.2H_2O = \underset{\text{Magnesite}}{1.8MgCO_3} + \underset{\text{Magnetite}}{0.1Fe_2O_3} + \underset{\text{Quartz}}{SiO_2} + 0.1CH_4 \quad (20)$$

Such reactions are of particular interest as they could produce an energy source for microbes and/or anthroprogenic activities. These reactions tend to be thermodynamically favorable at temperatures less than ~315 °C (McCollom and Bach, 2009). Conversely, at temperatures below ~150 °C, these reactions appear to be limited by slow reaction kinetics and partitioning of Fe(II) into brucite. McCollom and Bach (2009) estimated that the peak temperatures for H_2 production from reactions such as Eq. (19) are 200–315 °C. McCollom and Donaldson (2016), however reported that in the absence of catalysts, olivine dissolution generates little to no hydrogen or methane. In contrast, Neubeck et al. (2014) reported that although no H_2 production was observed in experiments performed at 30 to 50 °C, measurable quantities of H_2 were produced during the dissolution of forsterite in experiments performed at 70 °C in carbonate rich aqueous solutions in experiments lasting over 300 days. Reactions to form H_2 or CH_4 during olivine dissolution appear to be favored by the presence of magnetite, chromite or and/or other metal-rich minerals on the surface of olivine (Neubeck et al., 2011; Etiope et al., 2013, 2017). Miller et al. (2017) reported measurable production of H_2 during the interaction of partially serpentinized Oman dunite in both artificial rainwater and artificial seawater at 100 °C during experiments that lasted only 9 months. The origin of the produced H_2, however, was attributed to the presence of Fe^{2+} in the original brucite present in the rock rather than from the abundant forsterite. Nevertheless reactions such as Eq. (20) have the potential to both store carbon dioxide and provide carbon neutral hydrocarbons if sufficiently fast reaction pathways can be found.

4.4. Comparison of olivine dissolution rates and mechanisms with other silicate minerals

Although it is commonly believed that forsterite dissolution rates are always far faster than those of most other silicate minerals, this is somewhat a misconception owing to its relatively rapid dissolution rates in acidic conditions. In contrast to quartz and many aluminosilicate minerals, which exhibit dissolution rates that minimize as a function of pH then increase with increasing pH at basic conditions, the dissolution rates of forsterite decrease continuously with increasing pH. As such, forsterite forward dissolutions rates may be slower than those of many rock-forming aluminosilicates at basic pH. For example, the dissolution rates of forsterite are compared with those of quartz and albite in Fig. 13. Although forsterite dissolution rates are 3 to 5 orders of magnitude faster than those of albite and quartz at acidic pH, they differ by < 1.5 orders of magnitude at pH 9, and are slower than those of quartz and albite at pH > 11. Such variations led Gudbrandsson et al. (2011) to conclude that the liberation of divalent metals from crystalline basalt is dominated by olivine dissolution at acidic and neutral conditions, but by plagioclase dissolution at basic conditions.

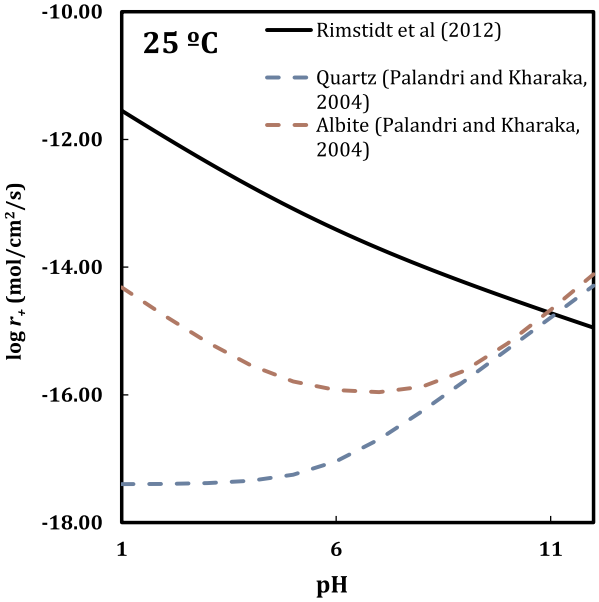

Fig. 13. Comparison of the forsterite forward dissolution rates, as calculated using equations and parameters reported by Rimstidt et al. (2012) with those of albite and quartz, as calculated using equations and parameters reported by Palandri and Kharaka (2004) as a function of pH at 25 °C.

The only parameters that alter substantially forsterite forward dissolution rates are pH, water activity, mineral-fluid interfacial surface area, and at neutral to basic conditions, the presence of some organic ligands. Factors such as the concentration of inorganic ligands and the presence of bacteria have appear to have relatively little effect aside from their role in changing pH and surface area, and complexing released iron. This behavior contrasts dramatically with that observed for other multi-oxide silicates, which have forward dissolution rates that are substantially affected by the presence of inorganic species including Al and Si (e.g. Oelkers et al., 1994, 2008b; Oelkers, 2001a; Schott et al., 2009) as well as the concentration of organic ligands (e.g. Ganor et al., 2009). Note, that the effect of aqueous organic ligands on the dissolution rates of many multi-oxide silicate minerals may largely stem from their influence on the aqueous activity of aluminum or other metal species that directly affect their rates (Oelkers and Schott, 1998). The origin of such effects on many multi-oxide silicate dissolution rates appears to be the need to break more than one distinct metal-oxygen bond in their structure to complete their dissolution (Oelkers et al., 1994; Oelkers, 2001a; Schott et al., 2009). This contrasts with the dissolution mechanism of the olivine minerals, which as described above requires the breaking of the ionic divalent metal-oxygen bonds in its structure. The dramatic difference in the dissolution rates of the various olivine minerals, which span over 6 orders of magnitude depending on the identity of the divalent metal in its structure, also provides insight into the dissolution mechanisms of those multi-oxide minerals, which require the breaking of several bonds. As the breaking

of distinct metal oxygen bonds in a mineral can proceed at rates that differ by orders of magnitude, the more rapidly reacting metals at or near the mineral surface can readily equilibrate with the aqueous solution before the more slowly reacting metals are liberated completing the overall dissolution of a mineral (cf. Oelkers et al., 2009).

5. Conclusions and perspectives

The results summarized above illustrate the consistency of the various past studies to describe the dissolution behavior of the olivines. This consistency provides insight into the processes controlling this reaction. Notably, constant temperature olivine forward dissolution rates are only influenced greatly by 1) pH, 2) water activity, 3) mineral-fluid interfacial surface area, and some organic ligands at neutral to basic conditions. Evidence suggests that the effects of aqueous inorganic and many organic species are limited, and may often be attributed to their influence on aqueous solution pH. The measured lowering of rates due to the presence of mineral coatings, as well as due to the presence of microbes can be attributed to their ability to decrease olivine surface area directly exposed to the reactive aqueous fluid. Some additional influence could be attributed to the effect microbes have on the oxidation and/or complexation of aqueous iron. Even in the absence of inorganic and organic coatings, the surface area normalized dissolution rates of olivine will tend to decrease with time, as olivine dissolution rates are spatially heterogeneous. As a consequence, the olivine surface will tend to be dominated by an increasingly less reactive surface with time as it dissolves. In the current state of knowledge, there are no evident pathways to accelerate greatly forsterite dissolution rates, other than increasing greatly its surface area or reacting it in extremely acidic conditions. As such its application to either enhanced weathering efforts, or the low temperature generation of hydrogen or hydrocarbons via the oxidation of its divalent iron is limited at present.

The present communication illustrates that current knowledge of olivine dissolution kinetics is far advanced compared to many other common multi-oxide silicate minerals. What is less advanced is our understanding of how the differences in the structure of these other silicate minerals compared to that of olivine results in their differing dissolution behavior as a function of aqueous fluid composition. Such research would be a major next step in allowing the more accurate temporal description of natural geochemical processes at and near the Earth's surface.

Acknowledgements

We thank Oleg Pokrovsky, Anna Harrison Vasillis Mavromatis, Martin Voigt, Chiara Marieni, Fieke Munders, and Lisa Fuellenbach for helpful discussions and encouragement. We would also like to thank Roy Wolgelius and Don Rimstidt for helpful reviews. This study has been supported by the Centre National de la Recherche Scientifique (CNRS), and the European Commission through projects CO2-REACT (MC-ITN-317235), CarbFix (EC coordinated action 283148), Min-GRO (MC-RTN-35488), and CarbFix2 (European Union's Horizon 2020 research and innovation programme under grant number 764760).

References

Aagaard, P., Helgeson, H.C., 1977. Thermodynamic and kinetic constraints on the dissolution of feldspars. Geol. Soc. Am. Abstr. Programs 9, 873.
Aagaard, P., Helgeson, H.C., 1982. Thermodynamic and kinetic constraints on reaction-rates among minerals and aqueous solutions. 1. Theoretical considerations. Am. J. Sci. 282, 237–285.
Agrawal, A.K., Mehra, A., 2016. Olivine dissolution from Indian dunite in saline water. Environ. Sci. Pollut. Res. 23, 22331–22339.
Awad, A., van Groos, A.F.K., Guggenheim, S., 2000. Forsteritic olivine: effect of crystallographic direction on dissolution kinetics. Geochim. Cosmochim. Acta 64, 1765–1772.
Bailey, A., 1974. Effect of temperature on the reaction of silicates with aqueous solutions in the low temperature range. In: First International Symposium on Water-Rock Interactions. 1976, Praha, pp. 375–380.
Bandstra, J.Z., Brantley, S.L., 2008. Surface evolution of dissolving minerals investigated with kinetic Ising model. Geochim. Cosmochim. Acta 72, 2587–2600.
Banfield, J.F., Velbel, D.R., Jones, B.F., 1990. Transmission electron microscopy of subsolidus oxidation and weathering of olivine. Contrib. Mineral. Petrol. 106, 110–123.
Bearat, H., McKelvy, M.J., Chizmeshya, A.V.G., Gormley, D., Nunez, R., Carpenter, R.W., Squires, K., Wolf, G.H., 2006. Carbon sequestration via aqueous olivine mineral carbonation: role of passivating layer formation. Environ. Sci. Technol. 15, 4802–4808.
Beinlich, A., Austrheim, H., 2012. In situ sequestration of atmospheric CO_2 at low temperature and surface cracking of serpentinized peridotite in mine shafts. Chem. Geol. 332, 32–44.
Beinlich, A., Mavromatis, V., Austrheim, H., Oelkers, E.H., 2014. Inter-mineral Mg isotope fractionation during hydrothermal ultramafic rock alteration – implications for natural water compositions. Earth Planet. Sci. Lett. 392, 166–176.
Berger, G., Cadoré, E., Schott, J., Dove, P., 1994. Dissolution rates of quartz in lead and sodium electrolyte solutions between 25 and 300 °C. Effect of the nature of surface complexes and reaction affinity. Geochim. Cosmochim. Acta 58, 541–551.
Berninger, U.-N., Jordan, G., Schott, J., Oelkers, E.H., 2014. The experimental determination of hydromagnesite precipitation rates at 22.5 to 75 °C. Min. Mag. 78, 1405–1416.
Black, J.R., Epstein, E., Rains, W.D., Yin, Q.Z., Casey, W.H., 2008. Magnesium-isotope fractionation during plant growth. Environ. Sci. Technol. 42, 7831–7836.
Blum, A.E., Lasaga, A.C., 1988. Role of surface speciation in the low-temperature dissolution of minerals. Nature 331, 431–433.
Bolou-Bi, E.B., Poszwa, A., Leyval, C., Vigier, N., 2010. Experimental determination of magnesium isotope fractionation during higher plant growth. Geochim. Cosmochim. Acta 74, 2523–2537.
Bonfils, B., Julcour-Lebigue, C., Guyot, F., Bodenan, F., Chiquet, P., Bourgeois, F., 2012. Comprehensive analysis of direct aqueous mineral carbonation using dissolution enhancing organic additives. Int. J. Greenhouse Gas Cont. 9, 334–346.
Brady, P.V., Walther, J.V., 1989. Controls on silicate dissolution rates in neutral and basic pH solutions at 25 °C. Geochim. Cosmochim. Acta 53, 2823–2830.
Brantley, S.L., 2008. Kinetics of mineral dissolution. In: Brantley, S.L., Kubici, J., White, A. (Eds.), Kinetics of Water-Rock Interaction. Spriger, New York, pp. 151–210.
Brantley, S.L., Mellott, N.P., 2000. Surface area and porosity of primary silicate minerals. Am. Mineral. 85, 1767–1783.
Brown, G.E., 1980. Olivines and silicate spinels. Rev. Mineral. Geochem. 5, 275–381.
Brunauer, S., Emmett, P.H., Teller, F., 1938. Adsorption of gases in multimolecular layers. J. Am. Chem. Soc. 60, 309–319.
Bundeleva, I.A., Menez, B., Auge, T., Bodenan, F., Recham, N., Guyot, F., 2014. Effect of cyanobacteria *Synechoccus* PCC 7942 on carbonation kinetics of olivine at 20 °C. Miner. Eng. 59, 2–11.
Cai, L., Xiao, H.-R., Huang, S.-M., Zhou, G.-T., 2013. Solubilization of magnesium-bearing silicate minerals and the subsequent formation of glushinskite by *Aspergillus niger*. Geomicrobiol J. 30, 302–312.
Cailleteau, C., Angeli, F., Devreux, F., Gin, S., Jestin, J., Jollivet, P., Spalla, O., 2008. Insight into silicate-glass corrosion mechanisms. Nat. Mater. 7, 978–983.
Case, D.H., Wang, F., Giammar, D.E., 2011. Precipitation of magnesium carbonates as a function of temperature, solution composition, and presence of silicate mineral substrate. Environ. Eng. Sci. 28, 881–889.
Casey, W.H., 1991. On the relative dissolution rates of some oxide and orthosilicate minerals. J. Colloid Interface Sci. 146, 586–589.
Casey, W.H., Sposito, G., 1993. On the temperature dependence of mineral reaction rates. Geochim. Cosmochim. Acta 56, 3825–3830.
Casey, W.H., Westrich, H., 1992. Control of dissolution rates of orthosilicate minerals by divalent metal–oxygen bonds. Nature 355, 157–159.
Casey, W.H., Westrich, H., Arnold, G.W., 1988. Surface chemistry of labradorite feldspar reacted with aqueous solutions at pH = 2, 3, and 12. Geochim. Cosmochim. Acta 53, 821–832.
Casey, W.H., Hochella Jr., M.F., Westrich, H.R., 1993a. Surface chemistry of manganiferous silicate minerals as inferred from experiments on tephroite (Mn_2SiO_4). Geochim. Cosmochim. Acta 57, 785–793.
Casey, W.H., Westrich, H.R., Banfield, J.F., Ferruzi, G., Arnold, G.W., 1993b. Leaching and reconstruction at the surfaces of dissolving chain-silicate minerals. Nature 366, 253–255.
Chen, Y., Brantley, S.L., 2000. Dissolution of forsteritic olivine at 65 °C and 2 < pH < 5. Chem. Geol. 165, 267–281.
Chou, L., Wollast, R., 1985. Steady-state kinetics and dissolution mechanisms of albite. Am. J. Sci. 285, 963–993.
Crundwell, R.K., 2014. The mechanism of dissolution of forsterite, olivine and minerals of the orthosilicate group. Hydrometallurgy 150, 68–82.
Cubillas, P., Köhler, S., Prieto, M., Causserand, C., Oelkers, E.H., 2005. How do mineral coatings affect dissolution rates? An experimental study of coupled $CaCO_3$ dissolution – $CdCO_3$ precipitation. Geochim. Cosmochim. Acta 69, 5459–5476.
Daux, V., Guy, C., Advocat, T., Crovisier, J.L., Stille, P., 1997. Kinetic aspects of basaltic fglass dissolution at 90 °C; role of aqueous silicon and aluminium. Chem. Geol. 265, 109–126.
Daval, D., Sissmann, O., Menguy, N., Saldi, G.D., Guyot, F., Martinez, I., Corvisier, J., Garcia, B., Machouk, I., Knauss, K.G., Hellmann, R., 2011. Influence of amorphous silica layer formation on the dissolution rate of olivine at 90 °C and elevated pCO_2. Chem. Geol. 284, 193–209.
Daval, D., Hellmann, R., Saldi, G.D., Wirth, R., Knauss, K.G., 2013. Linking nm-scale measurements of the anisotropy of silicate surface reactivity to macroscopic dissolution rate laws: new insights based on diopside. Geochim. Cosmochim. Acta 107,

121–134.
Davis, M.C., Brouwer, W.J., Wesolowsli, D.J., Anovitz, L.M., Lipton, A.S., Mueller, K.T., 2009. Magnesium silicate dissolution investigated by Si^{29} MAS, H^1-Si^{29} COMAS, Mg^{25} QCPMG, and H^1Mg^{25} CP QCPMG NMR. Phys. Chem. Chem. Phys. 11 (7013-1021).
Declercq, J., Bosc, O., Oelkers, E.H., 2013. Do organic ligands affect forsterite dissolution? Appl. Geochem. 39, 69–77.
Dehouck, E., Gaudin, A., Mangold, N., Lajaunie, L., Dauzeres, A., Grauby, O., Le Menn, E., 2014. Weathering of olivine under CO_2 atmosphere: a Martian perspective. Geochim. Cosmochim. Acta 135, 170–189.
Dufaud, F., Martinez, I., Shilobreeva, S., 2009. Experimental study of Mg-rich silicates carbonation at 400 and 500 °C and 1 kbar. Chem. Geol. 265, 79–87.
Eggleton, R.A., 1984. Formation of iddingsite rims on olivine: a transmission electron microscope study. Clay Clay Miner. 32, 1–11.
Eriksson, E., 1982. On the rate of dissolution of olivine in aqueous solutions. Vatten 38, 409–415.
Etiope, G., Ehlmann, B.L., Scholl, M., 2013. Low temperature production of exhalation of methane from serpentinized rocks on Earth: a potential analog for methane production on Mars. Icarus 224, 276–285.
Etiope, G., Samardzic, N., Grassa, F., Hrvatovic, H., Miosic, N., Skopljak, F., 2017. Methane and hydrogen in hyperalkaline groundwaters if serpentinized Dinaride ohiolite belt, Bosnia and Herzegovina. Appl. Geochem. 84, 286–296.
Felmy, A.R., Kafoku, O., Arey, B.W., Hu, J.Z., Hu, M., Schaef, H.T., Ilton, E.S., Hess, N.J., Pearce, C.I., Feng, J., Rosso, K.M., 2012. Reaction of water-saturated supercritical CO_2 with forsterite. Evidence for magnesite formation at low temperatures. Geochim. Cosmochim. Acta 91, 271–282.
Fischer, C., Arvidson, R.S., Luttge, A., 2012. How predictable are dissolution rates of crystalline material? Geochim. Cosmochim. Acta 98, 177–185.
Ganor, J., Reznik, I.J., Rosenberg, Y.O., 2009. Organics in water-rock interaction. Rev. Mineral. Geochem. 70, 259–369.
Garcia, B., Beaumont, V., Perfetti, E., Rouchon, V., Blanchet, D., Oger, P., Dromary, G., Huc, A.Y., Haeseler, F., 2010. Experimental and geochemical modelling of CO_2 sequestration by olivine: potential, quantification. Appl. Geochem. 25, 216–227.
Garcia, B., Lemelle, L., Rose-Koga, E., Perriat, P., Basset, R., Gillet, P., Albarede, F., 2013. An experimental model approach of biologically assisted silicate dissolution with olivine and *Escherichia coli* - impact on chemical weathering of mafic and atmospheric CO_2 drawdown. Appl. Geochem. 31, 216–227.
Gautier, J.-M., Oelkers, E.H., Schott, J., 2001. Are quartz dissolution rates proportional to BET surface areas? Geochim. Cosmochim. Acta 65, 1059–1070.
Gautier, Q., Bénézeth, P., Mavromatis, V., Schott, J., 2014. Hydromagnesite solubility product and growth kinetics in aqueous solution from 25 to 75 °C. Geochim. Cosmochim. Acta 138, 1–20.
Giammar, D.E., Bruant, R.G., Peters, C.A., 2005. Forsterite dissolution and magnesite precipitation at conditions relevant for deep saline aquifer storage and sequestration of carbon dioxide. Chem. Geol. 217, 257–276.
Gislason, S.R., Oelkers, E.H., 2003. Mechanism, rates, and consequences of basaltic glass dissolution: II. An experimental study of the dissolution rates of basaltic glass as a function of pH and temperature. Geochim. Cosmochim. Acta 67, 3817–3832.
Gislason, S.R., Oelkers, E.H., 2014. Carbon storage in basalt. Science 344, 373–374.
Golubev, S.V., Pokovsky, O.S., Schott, J., 2005. Experimental determination of the effect of dissolved CO_2 on the dissolution kinetics of Mg and Ca silicates at 25 °C. Chem. Geol. 217, 227–238.
Grambow, B., 1985. A general rate equation for nuclear waste glass corrosion. Mater. Res. Symp. Proc. 44, 15–27.
Grambow, B., Muller, R., 2001. First-order dissolution rate law and the role of surface layers in glass performance assessment. J. Nucl. Mater. 298, 112–124.
Grandstaff, D.E., 1978. Changes in surface area and morphology and the mechanism of forsterite dissolution. Geochim. Cosmochim. Acta 42, 1899–1901.
Grandstaff, D.E., 1986. The dissolution rate of forsteritic olivine from Hawaiian beach sand. In: Colman, S.M., Dethier, D.P. (Eds.), Rates of Chemical Weathering of Rocks and Minerals. Academic Press, Orlando, FL, pp. 41–57.
Griffioen, J., 2017. Enhanced weathering of olivine in seawater: the efficiency as revealed by thermodynamic scenario analysis. Sci. Total Environ. 575, 536–544.
Gudbrandsson, S., Wolff-Boenisch, D., Gislason, S.R., Oelkers, E.H., 2011. An experimental study of crystalline basalt dissolution from $2 <= pH <= 11$ and temperatures from 5 to 75 °C. Geochim. Cosmochim. Acta 75, 5496–5509.
Guyot, F., Daval, D., Dupraz, S., Martinez, I., Menez, B., Sissmann, O., 2011. CO_2 geological storage: the environmental mineralogy perspective. Compt. Rendus Geosci. 343, 246–259.
Hänchen, M., Prigiobbe, V., Storti, G., Seward, T.M., Mazotti, M., 2006. Dissolution kinetics of forsteritic olivine at 90–150 °C including effects of the presence of CO_2. Geochim. Cosmochim. Acta 70, 4403–4416.
Hangx, S.J., Spiers, C.J., 2009. Coastal spreading of olivine to control atmospheric CO_2 concentrations: a critical analysis of viability. Int. J. Greenh. Gas Con. 3, 757–777.
Hartmann, J., West, A.J., Renforth, P., Kohler, P., De LaRocha, C.L., Wolf-Gladrow, D.A., Durr, H.H., Scheffran, J., 2013. Enhanced weathering as a geoengineering solution to reduce carbon dioxide, supply nutrients, and mitigate ocean acidification. Rev. Geophys. 51, 113–149.
Haug, A.H., Kleiv, R.A., Munz, I.A., 2010. Investigating dissolution of mechanically activated olivine for carbonation purposes. Appl. Geochem. 25, 1547–1563.
Hausrath, E.M., Brantley, S.L., 2010. Basalt and olivine dissolution under cold, salty, and acidic conditions; what can we learn about recent aqueous weathering on Mars. J. Geophys. Res. 155. https://doi.org/10.1029/2010JE003610.
Hausrath, E.M., Treiman, A.H., Vicenzi, E., Bish, D.L., Blake, D., Sarrazin, P., Hoehler, T., Midtkandal, I., Steele, A., Brantley, S.L., 2008. Short- and long-term olivine weathering in Svalbard: implications for Mars. Astrobiology 8, 10790–11092.
Hellevang, H., Huang, S., Thouseth, I.H., 2011. The potential for low-temperature abiotic hydrogen generation and a hydrogen-driven deep biosphere. Astrobiology 11, 711–724.
Hodson, M.E., 2003. The influence of Fe-rich coatings on the dissolution of anorthite at pH 2.6. Geochim. Cosmochim. Acta 67, 3355–3363.
Hopkinson, L., Kristova, P., Rutt, K., Cressey, G., 2012. Phase transition in the system MgO-CO_2-H_2O during CO_2 degassing of Mg-bearing solutions. Geochim. Cosmochim. Acta 76, 1–13.
Hövelmann, J., Austrheim, H., Jamtveit, B., 2012. Microstructure and porosity evolution during experimental carbonation of a natural peridotite. Chem. Geol. 334, 254–265.
Huang, K.J., Teng, F.Z., Wei, G.J., Ma, J.L., Bao, Z.Y., 2012. Adsorption- and desorption-controlled magnesium isotope fractionation during extreme weathering of basalt in Hainan Island, China. Earth Planet. Sci. Lett. 359, 73–83.
Ilina, S.M., Viers, J., Lapitsky, S.A., Mialle, S., Mavromatis, V., Chmeleff, J., Brunet, P., Alekhin, Y.V., Isnard, H., Pokrovsky, O.S., 2013. Stable (Cu, Mg) and radiogenic (Sr, Nd) isotope fractionation in colloids of boreal organic-rich waters. Chem. Geol. 342, 63–75.
Jarvis, K., Carpenter, R.W., Windman, T., Kim, Y., Nunez, R., Alawneh, F., 2009. Reaction mechanisms for enhancing mineral sequestration of CO_2. Environ. Sci. Technol. 43, 6314–6319.
Johnson, N.C., Burt, T., Maher, K., Rosenbauer, R.J., Bird, D., Brown, G.E., 2014. Olivine dissolution and carbonation under conditions relevant for in-situ carbon storage. Chem. Geol. 373, 93–105.
Jonckbloedt, R.C.L., 1997. Olivine dissolution in sulphuric acid at elevated temperatures – implications for the olivine process, an alternative waste acid neutralizing process. J. Geochem. Explor. 62, 337–346.
King, H.E., Plümper, O., Putnis, A., 2010. Effect of secondary phase formation on the carbonation of olivine. Environ. Sci. Technol. 44, 6503–6509.
King, H.E., Plümper, O., Geisler, T., Putnis, A., 2011. Experimental investigation into the silicification of olivine: implications for the reaction mechanism and acid neutralization. Am. Mineral. 96, 1503–1511.
King, H.E., Satoh, H., Tsukamoto, K., Putnis, A., 2014. Surface-specific measurements of olivine dissolution by phase-shift interferometry. Am. Mineral. 99, 377–386.
Klien, F., Garrido, C.J., 2011. Thermodynamic constraints on mineral carbonation of serpentinized peridotite. Lithos 126, 147–160.
Kohler, S.J., Bosbach, D., Oelkers, E.H., 2005. Do clay mineral dissoltuion rates reach steady state? Geochim. Cosmochim. Acta 69, 1997–2006.
Kohler, P., Hartmann, J., Wolf-Gladrow, D.A., 2010. Geoengineering potential of artificially enhanced silicate weathering of olivine. PNAS 107, 20228–20233.
Kohler, P., Abrams, J.F., Voelker, C., Hauck, J., Wolf-Gladrow, D.A., 2013. Geoengineering impact of open ocean dissolution of olivine on atmospheric CO_2, surface ocean pH, and marine biology. Environ. Res. Lett. 8, 014009.
Lasaga, A.C., 1981. Transition state theory. Rev. Mineral. 8, 135–169.
Li, W.Y., Teng, F.Z., Ke, S., Rudnick, R.L., Gao, S., Wu, F.Y., Chappell, B.W., 2010. Heterogeneous magnesium isotopic composition of the upper continental crust. Geochim. Cosmochim. Acta 74, 6867–6884.
Li, Z.-J., Guo, J.-L., Dong, Z., Chen, J.-W., 2018. Insight into interactions of olivine-scCO_2-water system at 140 °C and 15 MPa during CO_2 mineral sequestration. Geosci. Front. https://doi.org/10.1016/j.gsf2017.12.008.
Lin, C.-C., Shen, P., 1993. Directional dissolution kinetics of willemite. Geochim. Cosmochim. Acta 57, 27–35.
Liu, Y., Olsen, A.A., Rimstidt, J.D., 2006. Mechanism for the dissolution of olivine series mineral in acidic solutions. Am. Mineral. 91, 455–458.
Luce, R.W., Bartlett, R.W., Parks, G.A., 1972. Dissolution kinetics of magnesium silicates. Geochim. Cosmochim. Acta 36, 35–50.
Luttge, A., Arvidson, R.S., Fisher, C., 2013. A stochastic treatment of crystal dissolution kinetics. Elements 9, 183–188.
Maher, K., Johnson, N.C., Jackson, A., Lammers, L.N., Torchinsky, A.B., Weaver, K.L., Bird, D.K., Brown, G.E., 2016. A spatially resolved surface kinetic model for forsterite dissolution. Geochim. Cosmochim. Acta 174, 313–334.
Marini, L., 2006. Geological Sequestration of Carbon Dioxide: Thermodynamics, Kinetics, and Reaction Path Modeling. Elsevier, Amsterdam (470 pp.).
Martinez, R.E., Weber, S., Bucher, K., 2014. Quantifying the kinetics of olivine dissolution in partially closed batch reactor systems. Chem. Geol. 367, 1–12.
Matter, J.M., Kelemen, P.B., 2009. Permanent storage of carbon dioxide in geological reservoirs by mineral carbonation. Nat. Geosci. 2, 837–842.
Matter, J.M., Takahashi, T., Goldberg, D., 2007. Experimental evaluation of in-situ CO_2-water-rock reactions during CO_2 injection in basaltic rocks: implications for geological CO_2 sequestration. Geochem. Geophys. Geosyst. 8.
Mavromatis, V., Pearce, C.R., Shirokova, L.S., Bundeleva, I.A., Pokrovsky, O.S., Benezeth, P., Oelkers, E.H., 2012. Magnesium isotope fractionation during hydrous magnesium carbonate precipitation with and without cyanobacteria. Geochim. Cosmochim. Acta 76, 161–174.
Mavromatis, V., Meister, P., Oelkers, E.H., 2014. Using stable isotopes to distinguish dolomite formations mechanisms: a case study from the Peru Margin. Chem. Geol. 385, 84–91.
McCollom, T.M., Bach, W., 2009. Thermodynamic constraints on hydrogen generation during the serpentinization of ultramafic rocks. Geochim. Cosmochim. Acta 73, 856–875.
McCollom, T.M., Donaldson, C., 2016. Generation of hydrogen and methane during experimental low-temperature reaction of ultramafic rocks with water. Astrobiology 16, 389–406.
Miller, H., Mayhew, L.E., Ellison, E.T., Kelemen, P., Kubo, M., Templeton, A.S., 2017. Low temperature hydrogen production during experimental hydration of partially serpentinized dunite. Geochim. Cosmochim. Acta 209, 161–183.
Montserrat, F., Renforth, P., Hartmann, J., Leermakers, M., Knops, P., Meysman, F.J.R., 2017. Olivine dissolution in seawater: implications for CO_2 sequestration through

enhanced weathering in costal environments. Environ. Sci. Technol. 51, 3960–3972.
Moosdorf, N., Renforth, P., Hartmann, J., 2014. Carbon dioxide efficiency of terrestrial enhanced weathering. Environ. Sci. Technol. 48, 4809–4816.
Morris, P.M., Wogelius, R.A., 2008. Phthalic acid complexation and the dissolution of forsteric glass studies via in situ FTIR and X-ray scattering. Geochim. Cosmochim. Acta 72, 1970–1985.
Murphy, W.M., Helgeson, H.C., 1987. Thermodynamic and kinetic constraints on reaction rates among minerals and aqueous solutions. III. Activated complexes and the pH-dependence of the rates of feldspar, pyroxene, wollastonite, and olivine hydrolysis. Geochim. Cosmochim. Acta 51, 3137–3153.
Murphy, W.M., Helgeson, H.C., 1989. Thermodynamic and kinetic constraints on reaction rates among minerals and aqueous solutions. IV. Retrieval of rate constants and activation parameters for the hydrolysis of pyroxene, wollastonite, olivine, analusite and quartz. Am. J. Sci. 288, 17–101.
Neubeck, A., Duc, N.T., Bastviken, D., Holm, N.G., 2011. Formation of H_2 and CH4 by weathering of olivine at temperatures between 30 and 70 °C. Geochem. Trans. 12, 6.
Neubeck, A., Duc, N.T., Hellevang, H., Oze, C., Bastviken, D., Bacsik, Z., Holm, N.G., 2014. Olivine alteration and H_2 production in carbonate-rich, low temperature aqueous environments. Planet. Space Sci. 96, 51–61.
Niles, P.B., Michalski, J., Ming, D.W., Golden, D.C., 2017. Elevated olivine weathering rates and cryogenic sulfate formation at cryogenic temperatures on Mars. Nat. Commun. 8. https://doi.org/10.1038/s41467-017-01227-7.
Oelkers, E.H., 2001a. General kinetic description of multioxide silicate mineral and glass dissolution. Geochim. Cosmochim. Acta 65, 3703–3719.
Oelkers, E.H., 2001b. An experimental study of forsterite dissolution rate as a function of temperature and aqueous Mg and Si concentration. Chem. Geol. 148, 485–494.
Oelkers, E.H., Schott, J., 1998. Does organic acid adsorption affect alkali-feldspar dissolution rates? Chem. Geol. 151, 235–245.
Oelkers, E.H., Schott, J., 1999. An experimental study of kyanite dissolution rates as a function of temperature and solution composition. Geochim. Cosmochim. Acta 63, 785–797.
Oelkers, E.H., Schott, J., 2001. An experimental study of enstatite dissolution rates as a function of pH, temperature, and aqueous Mg and Si concentration, and the mechanism of pyroxene/pyroxenoid dissolution. Geochim. Cosmochim. Acta 65, 1219–1231.
Oelkers, E.H., Schott, J., 2005. Geochemical aspects of CO_2 sequestration. Chem. Geol. 217, 183–186.
Oelkers, E.H., Schott, J., Devidal, J.-L., 1994. The effect of aluminum, pH, and chemical affinity on the rates of aluminosilicate dissolution reactions. Geochim. Cosmochim. Acta 58, 2011–2024.
Oelkers, E.H., Gislason, S.R., Matter, J., 2008a. Mineral carbonation of CO_2. Elements 4, 333–337.
Oelkers, E.H., Schott, J., Devidal, J.-L., 2008b. An experimental study of the dissolution mechanism and rates of muscovite. Geochim. Cosmochim. Acta 68 (14948-496).
Oelkers, E.H., Golubev, S.V., Chairat, C., Pokrovsky, O.S., Schott, J., 2009. The surface chemistry of multi-oxide silicates. Geochim. Cosmochim. Acta 73, 4617–4634.
Oelkers, E.H., Benning, L.G., Lutz, S., Mavromatis, V., Pearce, C.R., Plumper, O., 2015. The efficient long-term inhibition of forsterite dissolution by common soil bacteria and fungi at Earth surface conditions. Geochim. Cosmochim. Acta 168, 222–235.
Olsen, A.A., 2007. Forsterite Dissolution Kinetics: Applications and Implications for Chemical Weathering (Ph.D. Thesis). Virginia Tech University, Blacksburg, Virginia.
Olsen, A.A., Rimstidt, D., 2007. Using a mineral lifetime diagram to evaluate the persistence of olivine on Mars. Am. Mineral. 92, 598–602.
Olsen, A.A., Rimstidt, D., 2008. Oxalate promoted forsterite dissolution at low pH. Geochim. Cosmochim. Acta 72, 1758–1766.
Olsen, A.A., Hausrath, E.M., Rimstidt, J.D., 2015. Forsterite dissolution rates in Mg-sulfate-rich Mars analogue brines and implications for the aqueous history of Mars. J. Geophys. Res. Planets 120, 388–400.
Olsson, J., Bovet, N., Makovicky, E., Bechgaard, K., Balogh, Z., Stipp, S.L.S., 2012. Olivine reactivity with CO_2 and H_2O on a microscale: Implications for carbon sequestration. Geochim. Cosmochim. Acta 77, 86–97.
Opfergelt, S., Georg, R.B., Delvaux, B., Cabidoche, Y.M., Burton, K.W., Halliday, A.N., 2012. Mechanisms of magnesium isotope fractionation in volcanic soil weathering sequences, Guadeloupe. Earth Planet. Sci. Lett. 341, 176–185.
Opfergelt, S., Burton, K.W., Georg, R.B., West, A.J., Guicharnaud, R.A., Sigfusson, B., Siebert, C., Gislason, S.R., Halliday, A.N., 2014. Magnesium retention on the soil exchange complex controlling Mg isotope variations in soils, soil solutions and vegetation in volcanic soils, Iceland. Geochim. Cosmochim. Acta 125, 110–130.
Palandri, J.L., Kharaka, Y.K., 2004. A compilation of rate parameters of water-mineral interaction kinetics for application in geochemical modeling. In: U.S. Geological Survey, Open File Report 2004-1068.
Parkhurst, D.L., Appelo, C.A.J., 2013. Description of input and examples for PHREEQC version 3—a computer program for speciation, batch-reaction, one-dimensional transport, and inverse geochemical calculations. In: US Geological Survey.
Pearce, C.R., Saldi, G.D., Schott, J., Oelkers, E.H., 2012. Isotopic fractionation during congruent dissolution, precipitation and at equilibrium. Evidence from Mg isotopes. Geochim. Cosmochim. Acta 92, 170–183.
Plümper, O., Royne, A., Magraso, A., Jamtveit, B., 2012. The interface-scale mechanism of reaction-induced fracturing during serpentinization. Geology 40, 1103–1106.
Pogge von Strandmann, P.A.E., Burton, K.W., James, R.H., van Calsteren, P., Gislason, S.R., Sigfusson, B., 2008. The influence of weathering processes on riverine magnesium isotopes in a basaltic terrain. Earth Planet. Sci. Lett. 276, 187–197.
Pokrovsky, O.S., Schott, J., 2000a. Forsterite surface composition in aqueous solutions: a combined potentiometric, electrokinetic, and spectroscopic approach. Geochim. Cosmochim. Acta 64, 3299–3312.
Pokrovsky, O.S., Schott, J., 2000b. Kinetics and mechanism of forsterite dissolution at 25 °C and pH from 1 to 12. Geochim. Cosmochim. Acta 64, 3313–3325.
Pokrovsky, O.S., Schott, J., 2002. Surface chemistry and dissolution kinetics of divalent metal carbonates. Environ. Sci. Technol. 36, 426–432.
Pokrovsky, O.S., Golubev, S.V., Jordan, G., 2009. Effect of organic and inorganic ligands on calcite and magnesite dissolution. Chem. Geol. 265, 323–343.
Pollet-Villard, M., Daval, D., Ackerer, P., Saldi, G.D., Wild, B., Knauss, K.G., Fritz, B., 2016. Does crystallographic anisotropy prevent the conventional treatment of aqueous mineral reactivity? A case study based on K-feldspar dissolution kinetics. Geochim. Cosmochim. Acta 190, 294–308.
Prigiobbe, V., Costa, G., Baciocchi, R., Hänchen, M., Mazzotti, M., 2009. The effect of CO_2 and salinity on olivine dissolution kinetics at 120 °C. Chem. Eng. Sci. 64, 3510–3515.
Prikryl, J., Stefansson, A., Pearce, C.R., 2018. Tracing olivine carbonation and serpentinization in CO_2-rich fluids via magnesium exchange and isotopic fractionation. Geochim. Cosmochim. Acta. https://doi.org/10.1016/j.gca.2018.09.022. (in press).
Putnis, A., 1992. Introduction to Mineral Sciences. Cambridge University Press (457 pp.).
Putnis, A., 2009. Mineral replacement reactions. Rev. Mineral. Geochem. 70, 87–124.
Renforth, P., Pogge von Stransmann, P.A.E., Henderson, G.M., 2015. The dissolution of olivine added to soil: implications for enhanced weathering. Appl. Geochem. 61, 109–118.
Rigopoulos, I., Petallidou, K.C., Vasiliades, M.A., Delimitis, A., Ioannou, I., Efstathiou, A.M., Kyratsi, Th., 2015. Carbon dioxide storage in olivine basalts: effect of ball milling process. Powder Technol. 273, 220–229.
Rigopoulos, I., Vasiliades, M.A., Ioannou, I., Efstathiou, A.M., Godelitsas, A., Kyratsi, Th., 2016. Enhancing the rate of ex situ mineral carbonation in dunites. Adv. Powder Technol. 27, 360–371.
Rimstidt, J.D., Brantley, S.L., Olsen, A.A., 2012. Systematic review of forsterite dissolution rate data. Geochim. Cosmochim. Acta 99, 159–178.
Rigopoulos, I., Harrison, A.L., Delimitis, A., Ioannou, I., Efstathiou, A.M., Godelitsas, A., Kyratsi, Th., Oelkers, E.H., 2018. Carbon sequestration via enhanced weathering of peridotes and basalts in seawater. Appl. Geochem. 91, 197–207.
Rosso, J.J., Rimstidt, J.D., 2000. A high resolution study of forsterite dissolution rates. Geochim. Cosmochim. Acta 64, 797–811.
Ruiz-Agudo, E., Putnis, C.V., Rodriguez-Navarro, C., Putnis, A., 2012. Mechanism of leached layer formation during chemical weathering of silicate minerals. Geology 40, 947–950.
Saldi, G.D., Kohler, S.J., Marty, N., Oelkers, E.H., 2007. Dissolution rates of talc as a function of solution composition, pH and temperature. Geochim. Cosmochim. Acta 71, 3446–3457.
Saldi, G.D., Jordan, G., Schott, J., Oelkers, E.H., 2009. Magnesite growth rates as a function of temperature and saturation state. Geochim. Cosmochim. Acta 73, 5646–5657.
Saldi, G.D., Schott, J., Pokrovsky, O.S., Gautier, Q., Oelkers, E.H., 2012. An experimental study of magnesite precipitation rates at neutral to alkaline conditions and 100–200 °C as a function of pH, aqueous solution composition and chemical affinity. Geochim. Cosmochim. Acta 83, 93–109.
Saldi, G.D., Daval, D., Morvan, G., Knauss, K.G., 2013. The role of Fe and redox conditions in olivine carbonation rates: an experimental study of the rate limiting reactions at 90 and 150 °C in open and closed systems. Geochim. Cosmochim. Acta 118, 157–183.
Saldi, G.D., Daval, D., Guo, H., Guyot, F., Bernard, S., Le Guillou, C., Davis, J.A., Knauss, K.G., 2015. Mineralogical evolution of Fe–Si-rich layers at the olivine-water interface during carbonation reactions. Am. Mineral. 100, 2655–2669.
Sanemasa, I., Yoshida, L., Ozawa, T., 1972. The dissolution of olivine in aqueous solutions of inorganic acids. Bull. Chem. Soc. Jpn. 45, 1741–1746.
Santelli, C.M., Welch, S.A., Westrich, H.R., Banfield, J.F., 2001. Fe oxidizing bacteria and the weathering of Fe silicate minerals. Chem. Geol. 180, 99–115.
Schott, J., Berner, R.A., 1983. X-ray photoelectron studies of the mechanism of iron silicate dissolution during weathering. Geochim. Cosmochim. Acta 47, 2233–2240.
Schott, J., Berner, R.A., 1985. Dissolution mechanisms of proxenes and olivines during weathering. In: Drever, J.I. (Ed.), The Chemistry of Weathering. D. Reidel Publishing Company, pp. 35–53.
Schott, J., Oelkers, E.H., 1995. Dissolution and crystallization rates of silicate minerals as a function of chemical affinity. Pure Appl. Chem. 67, 903–910.
Schott, J., Pokrovsky, O.S., Oelkers, E.H., 2009. The link between mineral dissolution/precipitation kinetics and solution chemistry. Rev. Mineral. Geochem. 70, 207–258.
Schott, J., Pokrovsky, O.S., Spalla, O., Devreux, F., Gloter, A., Mielczarski, J.A., 2012. Formation, growth and transformation of leached layers during silicate minerals dissolution: the example of wollastonite. Geochim. Cosmochim. Acta 98, 259–281.
Schott, J., Mavromatis, V., Fujii, T., Pearce, C., Oelkers, E.H., 2016. The control of magnesium aqueous speciation on Mg isotope composition in carbonate minerals: theoretical and experimental modeling. Chem. Geol. 445, 120–134.
Schuiling, R.D., Krijgsman, P., 2006. Enhanced weathering: an effective and cheap tool to sequester CO_2. Clim. Chang. 74, 349–354.
Seiffert, F., Bandow, N., Bouchez, J., von Blackengurg, F., Gorbushina, A.A., 2014. Microbial colonization of bare rocks: laboratory biofilm enhances mineral weathering. Procedia Earth Planet. Sci. 10, 123–129.
Seyama, H., Soma, M., Tanaka, A., 1996. Surface characterization of acid-leached olivines by X-ray photoelectron spectroscopy. Chem. Geol. 129, 209–216.
Shirokova, L.S., Benezeth, P., Pokrovsky, O.S., Gerard, E., Menez, B., Alfredsson, H., 2012. Effect of the heterotrophic bacterium *Psuedomonas reactans* on olivine dissolution kinetics and implications for CO_2 storage in basalts. Geochim. Cosmochim. Acta 80, 30–50.
Shirokova, L.S., Mavromatis, V., Bundeleva, I.A., Pokrovsky, O.S., Benezeth, P., Gerard, E., Pearce, C.R., Oelkers, E.H., 2013. Using Mg isotopes to trace cyanobacterially mediated magnesium carbonate precipitation in alkaline lakes. Aquat. Geochem. 19, 1–24.
Siegel, D.I., Pfannkuch, H.O., 1984. Silicate mineral dissolution at pH 4 and near standard

temperature and pressure. Geochim. Cosmochim. Acta 48, 197–201.
Siever, R., Woodford, N., 1979. Dissolution kinetics and weathering of mafic minerals. Geochim. Cosmochim. Acta 43, 717–724.
Sissmann, O., Daval, D., Brunet, F., Guyot, F., Verlaguet, A., Pinquier, Y., Findling, N., Martinez, I., 2013. The deleterious effects of secondary phases on olivine carbonation yield: insight from time-resolved aqueous-fluid sampling and FIB-TEM characterization. Chem. Geol. 357, 186–202.
Sissmann, O., Brunet, F., Martinez, I., Guyot, F., Verlaguet, A., Pinquier, Y., Deval, D., 2014. Enhanced oliving carbonation within a basalt as compared to single-phase experiments: reevaluating the potential of CO_2 mineral sequestration. Environ. Sci. Technol. 48, 5512–5519.
Snaebjornsdottir, S.O., Gislason, S.R., Galcczka, I.M., Oelkers, E.H., 2018. Reaction path modelling of ion-situ mineralization of CO_2 at the CarbFix site at Hellisheidi, SW-Iceland. Geochim. Cosmochim. Acta 220, 348–366.
Stockmann, G.J., Wolff-Boenisch, D., Gislason, S.R., Oelkers, E.H., 2011. Do carbonate precipitates affect dissolution kinetics? 1: Basaltic glass. Chem. Geol. 284, 306–316.
Stockmann, G.J., Wolff-Boenisch, D., Gislason, S.R., Oelkers, E.H., 2013. Do carbonate precipitates affect dissolution kinetics? 2: Diopside. Chem. Geol. 337, 56–66.
Stockmann, G.J., Wolff-Boenisch, D., Bovet, N., Gislason, S.R., Oelkers, E.H., 2014. The role of silicate surfaces on calcite precipitation kinetics. Geochim. Cosmochim. Acta 135, 231–250.
Stopar, J.D., Taylor, G.J., Hamilton, V.E., Browning, L., 2006. Kinetic model of olivine dissolution and extent to aqueous alteration on Mars. Geochim. Cosmochim. Acta 70, 6036–6152.
Sugimori, H., Kanzaki, Y., Murakami, T., 2012. Relationships between Fe redistribution and P_{O2} during mineral dissolution under low O_2 conditions. Geochim. Cosmochim. Acta 84, 29–46.
Teng, F.-Z., Wadhwa, M., Helz, R.T., 2007. Investigation of magnesium isotope fractionation during basalt differentiation. Implications for a chondritic composition of the terrestrial mantle. Earth Planet. Sci. Lett. 261, 84–92.
Teng, F.Z., Li, W.Y., Rudnick, R.L., Gardner, L.R., 2010. Contrasting lithium and magnesium isotope fractionation during continental weathering. Earth Planet. Sci. Lett. 300, 63–71.
Terry, B., Monhemius, A.J., 1983. Acid dissolution of willemite ($(Zn,Mn)_2SiO_4$) and hemimorphite ($Zn_4Si_2O_7(OH)_2H_2O$). Metall. Trans. A. 14-B, 335–346.
Tipper, E.T., Galy, A., Gaillardet, J., Bickle, M.J., Elderfield, H., Carder, E.A., 2006. The magnesium isotope budget of the moden ocean: constraints from riverine magnesium isotope ratios. Earth Planet. Sci. Lett. 250, 241–253.
Tipper, E.T., Gaillardet, J., Louvat, P., Capmas, F., White, A.F., 2010. Mg isotope constraints on soil pore-fluid chemistry: evidence from Santa Cruz, California. Geochim. Cosmochim. Acta 74, 3883–3896.
Torres, M.A., West, A.J., Nealson, K., 2014. Microbial acceleration of olivine dissolution via siderophore production. Procedia Earth Planet. Sci. 10, 118–122.
Van Herk, J., Pietersen, H.S., Schuiling, R.D., 1989. Neutralization of industrial waste acids with olivine – the dissolution of forsteritic olivine at 40–70 °C. Chem. Geol. 76, 341–352.
Van Noort, R., Spiers, C.J., Drury, M.R., Kadianis, M.T., 2013. Peridote dissolution and carbonation rates at fracture surfaces under conditions relevant for in-situ mineralizaion of CO_2. Geochim. Cosmochim. Acta 106, 1–24.
Velbel, M.A., 1999. Bond strength and the relative weathering rates of simple orthosilicates. Am. J. Sci. 299, 679–696.
Velbel, M.A., 2009. Dissolution of olivine during natural weathering. Geochim. Cosmochim. Acta 73, 6098–6113.
Velbel, M.A., 2014. Etch pit size, dissolution rate, and time in the experimental dissolution of olivine: implications for estimating olivine lifetime at the surface of Mars. Am. Mineral. 99, 2227–2233.
Wang, F., Giammar, D.E., 2012. Forsterite dissolution in saline water at elevated temperature and high CO_2 pressure. Environ. Sci. Technol. 41, 168–173.
Wasklewicz, T., Dorn, R.I., Clark, S., Hetrick, J., Pope, G., Liu, T., Krinsley, D.H., Dixon, J., Moore, R.B., Clark, J., 1993. Olivine does not necessarily weather first. Singap. J. Trop. Geogr. 14, 72–80.
Weber, S., Martinez, R.E., 2017. Effects of *Synechococcus* sp. cyanobacteria inert biomass on olivine dissolution: implications for the application of enhanced weathering methods. Appl. Geochem. 84, 162–172.
Welch, S.A., Banfield, J.F., 2002. Modification of olivine surface morphology and reactivity by microbial activity during chemical weathering. Geochim. Cosmochim. Acta 66, 213–221.
Westrich, H.R., Cugan, R.T., Casey, W.H., Zemitis, C., Arnold, G.W., 1993. The dissolution kinetics of mixed-cation orthosilicate minerals. Am. J. Sci. 293, 869–893.
Wimpenny, J., Gislason, S.R., James, R.H., Gannoun, A., Pogge Von Strandmann, P.A.E., Burton, K.W., 2010. The behaviour of Li and Mg isotopes during primary phase dissolution and secondary mineral formation in basalt. Geochim. Cosmochim. Acta 74, 5259–5279.
Wogelius, R.A., Walther, J.V., 1991. Olivine dissolution at 25 °C: effects of pH, CO_2 and organic acids. Geochim. Cosmochim. Acta 55, 943–954.
Wogelius, R.A., Walther, J.V., 1992. Olivine dissolution kinetics at the near-surface conditions. Chem. Geol. 97, 101–112.
Xiong, W., Giammar, D.E., 2014. Forsterite carbonation in zones with transported limited by diffusion. Environ. Sci. Tech. Lett. 2014, 333–338.
Xiong, W., Wells, R.K., Giammar, D.E., 2017. Carbon sequestration in olivine and basalt powder packed beds. Environ. Sci. Technol. 51, 2105–2112.
Zakaznova-Herzog, V.P., Nesbitt, H.W., Bancroft, G.M., Tse, J.S., 2008. Characterization of leached layers on olivine and pyroxenes using high-resolution XPS and density functional calculations. Geochim. Cosmochim. Acta 72, 69–86.
Zhu, W., Fusseis, F., Lisabeth, H., Xing, T., Xiao, X., De Andrade, V., Karato, S.-I., 2016. Experimental evidence of reaction-induced fracturing during olivine carbonation. Geophys. Res. Lett. 43, 9535–9543. https://doi.org/10.1002/2016GL070834.